OFFICIAL

AMRL-TR-65-53



# INTERACTION BETWEEN AIR FLOW AND AIRBORNE SOUND IN A DUCT

*F. P. MECHEL*
*P. A. MERTENS*
*W. M. SCHILZ*

*III. PHYSIKALISCHES INSTITUT*
*DER UNIVERSITÄT GÖTTINGEN*

SEPTEMBER 1965

**Distribution of this document is unlimited.**




AEROSPACE MEDICAL RESEARCH LABORATORIES
AEROSPACE MEDICAL DIVISION
AIR FORCE SYSTEMS COMMAND
WRIGHT-PATTERSON AIR FORCE BASE, OHIO

## NOTICES

When US Government drawings, specifications, or other data are used for any purpose other than a definitely related Government procurement operation, the Government thereby incurs no responsibility nor any obligation whatsoever, and the fact that the Government may have formulated, furnished, or in any way supplied the said drawings, specifications, or other data, is not to be regarded by implication or otherwise, as in any manner licensing the holder or any other person or corporation, or conveying any rights or permission to manufacture, use, or sell any patented invention that may in any way be related thereto.

Requests for copies of this report should be directed to either of the addressees listed below, as applicable:

Federal Government agencies and their contractors registered with Defense Documentation Center (DDC):

DDC
Cameron Station
Alexandria, Virginia 22314

Non-DDC users (stock quantities are available for sale from):

Chief, Input Section
Clearinghouse for Federal Scientific & Technical Information (CFSTI)
Sills Building
5285 Port Royal Road
Springfield, Virginia 22151

Change of Address

Organizations and individuals receiving reports via the Aerospace Medical Research Laboratories automatic mailing lists should submit the addressograph plate stamp on the report envelope or refer to the code number when corresponding about change of address or cancellation.

Do not return this copy. Retain or destroy.

# INTERACTION BETWEEN AIR FLOW AND AIRBORNE SOUND IN A DUCT

*F. P. MECHEL*
*P. A. MERTENS*
*W. M. SCHILZ*

# Foreword

The information presented in this report was obtained by III. Physikalisches Institut der Universität Göttingen, Germany, under Contract No. AF 61(052)-666 for the Biodynamics and Bionics Division, Biophysics Laboratory, Aerospace Medical Research Laboratories, Aerospace Medical Division, Wright-Patterson AFB, Ohio. The studies were made in support of Project 7231, "Biomechanics of Aerospace Operation," and Task 723104, "Biodynamic Environments of Aerospace Flight Operations," under the supervision of Professor Dr. Erwin Meyer. Technical and administrative personnel monitoring this effort have included Dr. H. von Gierke, R. G. Powell, and J. N. Cole.

The investigations reported herein are part of a research program under Contract No. AF 61(052)-112 and resulted in four technical documentary reports, AMRL-TDR-62-140 (I), (II), (III), and (IV), entitled "Research on Sound Propagation in Sound-absorbent Ducts with Superimposed Air Streams." The studies covered by these reports were made during the period from June 1958 through January 1963. The present report covers the period from February 1963 through January 1964.

This technical report has been reviewed and is approved.

J. W. HEIM, PhD
Technical Director
Biophysics Laboratory
Aerospace Medical Research
Laboratories

# Abstract

Several studies of the interaction between air flow and airborne sound in a duct have been made. Three projects were investigated: (1) The excitation of boundary layer distortions in a laminar boundary layer by simulated oscillatory flexural waves was investigated. Results show boundary layer waves are excited whenever the phase velocity of the flexure wave is in the instability range of the phase velocity of boundary layer waves. (2) The propagation of a pressure pulse wave front and the acoustic impedance of porous absorbers are examined in ducts with air flow. Measurements prove the sound energy of the wave front is directed towards the walls and the absorber impedance becomes nonlinear when the absorber is penetrated by the flow. (3) The effect on the acoustic radiation impedance of an orifice with flow discharge restricted by fences and diaphragms was investigated. The acoustic resistance was shown to increase at low frequencies due to the restrictions.

# Table of Contents

# Table of Contents
(continued)

# List of Illustrations

# List of Illustrations
(continued)

# List of Symbols

**SECTION II.**

| | |
|---|---|
| x | coordinate in flow direction |
| A | elongation amplitude of oscillators perpendicular to surface |
| $A_s$ | threshold amplitudes |
| $\lambda$ | wavelength |
| $\lambda_o$ | wavelength of flexural wave |
| $\delta^*$ | displacement thickness |
| f | frequency |
| $f_s$ | signal frequency |
| $f_c$ | frequency of coincidence |
| $U\infty$ | flow velocity on the duct axis |
| $c_r$ | phase velocity of boundary layer wave |
| $\alpha$ | amplitude exponent of boundary layer wave in dB/cm |
| $c_r/U\infty$ | normalized phase velocity |
| $2\pi f\delta^*/U\infty$ | normalized frequency |
| Re | Reynolds number |
| $\phi$ | phase angle |
| Tu | turbulence level |

**SECTION III.**

| | |
|---|---|
| $A_v$ | nonlinearity coefficient |
| C | ray constant |
| $c_o$ | adiabatic sound velocity |
| L | travelling path of the first wave front |
| M(y) | Mach number |
| $r_o$ | flow resistance without stationary flow |
| $r_v$ | flow resistance with superimposed flow |
| x | coordinate parallel to the wall |
| y | coordinate perpendicular to the bottom of the duct |
| V | flow velocity |
| $\rho$ | density of air |
| $\Phi$ | wave function |

**SECTION IV.**

| | |
|---|---|
| a | radius of orifice |
| b | width of air jet |
| $c_o$ | sound velocity without flow |
| $c_1$ | downstream sound velocity |
| $c_2$ | upstream sound velocity |
| $d=\underline{p}_{min}/\underline{p}_{max}$ | pressure node ratio |
| f | frequency |

# List of Symbols
(continued)

| | |
|---|---|
| $j=(-1)^{1/2}$ | |
| $k_o$ | wavenumber without flow |
| $k_1$ | wavenumber for downstream propagation |
| $k_2$ | wavenumber for upstream propagation |
| $k_oa=2\pi fa/c_o$ | frequency parameter |
| $M=V/c_o$ | Mach number |
| $p$ | total pressure |
| $\Delta p$ | static pressure drop |
| $\underline{p}$ | sound pressure |
| $\overline{P}$ | static pressure |
| $q$ | surface coverage |
| $r$ | magnitude of reflection coefficient |
| $R$ | resistance of orifice |
| $Tu$ | turbulence level |
| $v$ | total velocity |
| $\underline{v}$ | acoustic particle velocity |
| $\overline{V}$ | flow velocity |
| $\overline{\overline{V}}$ | average flow velocity in the measuring tube |
| $V_{ax}$ | axial flow velocity |
| $\underline{W}=\underline{p}/\underline{v}$ | acoustic impedance of orifice |
| $x$ | coordinate in flow direction, origin in orifice |
| $\Delta x$ | distance of adjacent sound pressure minima |
| $x_{min}$ | position of sound pressure minimum nearest to orifice |
| $X$ | reactance of orifice |
| $y, z$ | coordinates perpendicular to flow direction |
| $Z=\rho c_o$ | characteristic impedance of air |
| $\lambda_o$ | acoustic wavelength without flow |
| $\rho$ | density of air |
| $\phi$ | phase of reflection coefficient |
| $\omega$ | angular frequency |

## SECTION I.
# Introduction

In previous measurements (ref. 13) the flow boundary layer of a flat plate was shown to be controlled by acoustical means at the stagnation point of the plate. Another point of interest is the possibility of acoustic boundary layer control not so much in the stagnation point but during the development of the boundary layer along the plate itself.

One method in this direction is the interference between the boundary layer waves, which are an intermediate status of the boundary layer between laminar and turbulent flows, and a deformation of the plate surface in the manner of a propagating flexural wave. It can be expected immediately that the interference will be strongest if both types of wave, i.e. the boundary layer wave and the flexural wave, propagate in the same direction and if their velocities of propagation are close together.

In the present report (Section II) some critical remarks are made concerning the development of flexural waves with the demanded phase velocities. The best method to generate a flexural wave of variable parameters proved to be the simulation of the surface deformations of a propagating flexural wave through periodically spaced narrow oscillators driven with a given phase lag. A smoothing of the amplitude distribution is obtained by a flexible foil stretched over the oscillators. Furthermore, the inertia of the changes in the boundary layer makes a wave out of punctual excitations periodically spaced.

The investigations of the sound propagation (ref. 13) in sound absorbing ducts with superimposed air flow have not answered the question of how the shape of the acoustic wave fronts are influenced by the gradient of the flow velocity. Another question in this connection is the existence of a stable wave front in ducts with lateral dimensions comparable with the wavelength. Measurements at low frequencies indicate the existence of such wave fronts of constant shape. It is not understood up to now which mechanism compensates for the different wave convection in different places of the flow velocity profile.

In order to get an insight into the superposition of wave components in the boundary layer which have run through different zones of flow velocities, the propagation of short pressure pulses in a duct with and without sound absorbers is studied.

Another topic covered in Section III is the influence of flow on the acoustic impedance of sound absorbers. In another Report (ref. 13, Vol III), a theory was given for the computation of the sound attenuation in absorbing ducts with superimposed air flow. The wall impedance of the absorbers in the presence of the flow entered into this theory. It is important, therefore, to know whether the impedance is affected by the flow, and if so how it could be evaluated from the normally known impedance, i.e., without flow.

Acoustical low pass filters are difficult to be realized. Therefore, it will be difficult to inhibit the sound to be radiated from a flow discharge orifice. The fraction of the radiated sound is determined by the radiation impedance of the orifice. With a tube, the diameter of which is small compared to the wavelength, this radiation impedance is the termination impedance of the tube. It can be determined from the standing wave pattern in the tube.

The measurements represented (Section IV) yielded a strong influence of the flow velocity upon the radiation impedance. Possible reasons for this influence are checked. Some of them, such as turbulence level in the tube or behind the orifice or the shape of the jet behind the orifice, proved to be rather ineffective while the drop of the static pressure across obstacles in the orifice sets up additional terms to the acoustic resistance of the orifice.

## SECTION II.

# Effects of Acoustic Excitation on the Flow Boundary Layer In Air

### EXPERIMENTAL SET-UP

The influence of the deformation of an otherwise plane wall by a propagating wave on the flow boundary layer has been investigated theoretically by several authors (refs. 2, 3). The present report especially deals with experimental investigations of the excitation of boundary layer distortions by such wall deformations.

The duct used for these measurements had the lateral dimensions of 10 x 10 $cm^2$ and allowed measurements in the flow velocity range from 5 to 40 m/sec. The turbulence level of the incoming flow on the duct axis is smaller than $4 \cdot 10^{-4}$%. Into this duct a flat plate with a sharp leading edge is mounted parallel to the flow. The central section of this plate could be replaced by sound generators or by flexural wave generators.

Without artificially induced distortions the boundary layer is laminar along the whole test section (about 50 cm). The boundary layer displacement thickness is between 0.3 and 0.5 mm.

The oscillations and the mean velocities in the boundary layer are measured by two hot-wire anemometers which can be moved parallel and perpendicular to the plate. The elongation amplitude of the wall oscillations are measured by capacitive probes (carrier-frequency method).

Preliminary experiments had shown that boundary layer distortions can be excited at rather small amplitudes ($A \approx 10^{-3}$ mm) with a pistonlike transducer inserted into the test plate. For more detailed investigations of the excitation of boundary layer distortions a wall oscillation was developed which corresponds to a surface flexural wave propagating in one direction. The phase velocity of this flexural wave has to be within the range of the phase velocities of the free boundary layer waves in order to get coincidence of the two waves. The phase velocity and the frequency of unstable boundary layer waves are, according to the theory by Tollmien and Schlichting (ref. 19), uniquely determined by the Reynolds number. From this and the dimensions of the duct the flexural wave generator should have a frequency range between 0.2 and 1.5 kcps and an associated range of wavelengths between 5 and 30 mm. Accordingly, the phase velocity of the bending wave should vary between 1 m/sec and 20 m/sec. These small velocities cannot be realized by a homogeneous material yielding at the same time satisfactory static stability and small absorption. By a system of coupled oscillators the requested small phase velocity could be obtained, the attenuation, however, was too great for practical applications.

Finally, an arrangement was chosen which samples the flexural wave at two points per wavelength. It consists of a plate with two sets of parallel slits which are covered by a thin foil on the side of the flow. Each set is driven by a pressure chamber loudspeaker in antiphase to each other. Thus each slit oscillates in opposite phase with respect to its neighbours. In the measurements reported below four systems with the double slit distance $\lambda_0 = 8$; 14; 20 and 28 mm were used. *Fig. 1* shows one of these systems.

The system in the test plate is a linear arrangement of oscillators in opposite phase to each other. Since their distance from each other is small compared to the acoustic wavelength, virtually no sound is radiated towards the sides of the system. The sound pressure decreases rapidly with increasing distance from the oscillators. A decrease of 20 dB/cm was measured.

The spatial distribution of phase and amplitude of the surface oscillations generated by the slits corresponds to that of a standing wave. Measurements of the velocity oscillations in the boundary layer above the oscillator system, however, yield the phase distribution of a propagat-

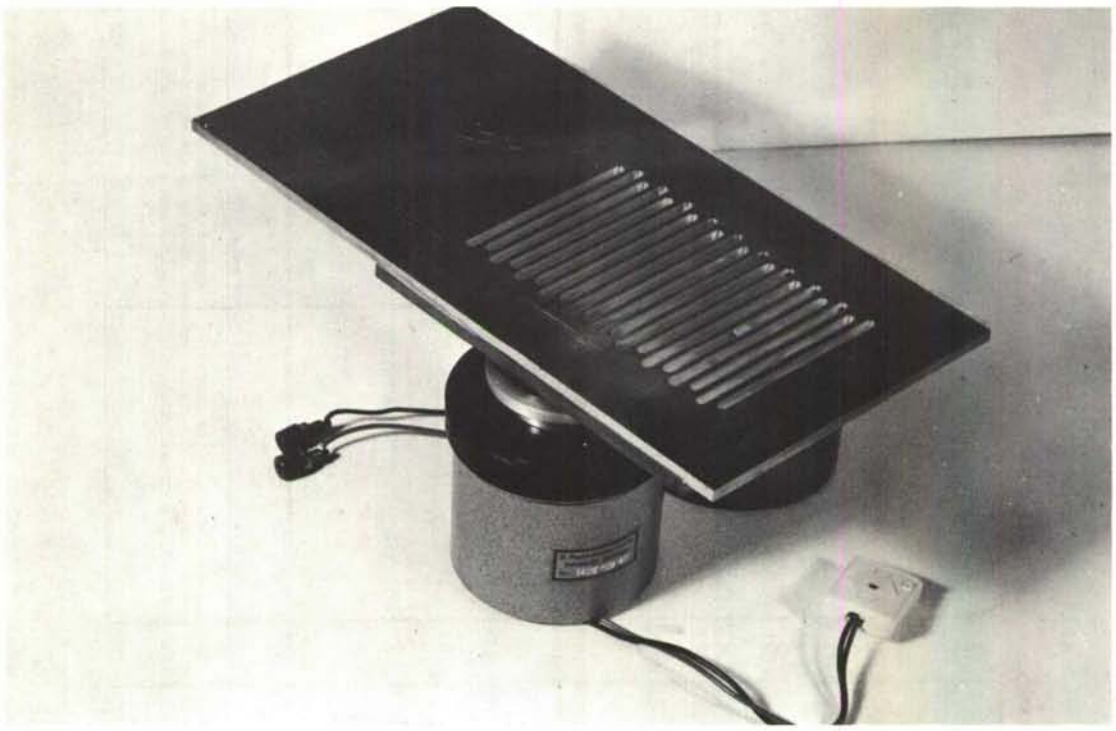

Fig. 1. View of driving system for flexural waves. $\lambda_o = 14$ mm.

ing wave. This effect is directly proportional to the flow velocity. In *Fig. 2* the phase measured along the test plate is presented for several flow velocities. Here the signal frequency is $f_s = 543$ cps, and the flow velocities are between 7 m/sec and 20 m/sec. The transition from a standing wave to a propagating wave can clearly be recognized.

## EXCITATION OF BOUNDARY LAYER WAVES IN COINCIDENCE

Further measurements have shown that even small elongation amplitudes of the surface lead to the onset of boundary layer waves which, in turn, lead to turbulence in the boundary layer. The induced boundary layer waves have the frequencies of the wall oscillations. *Fig. 3* shows how the oscillation velocities of the boundary layer wave develop from the level produced by the spatially periodic generating system. There the oscillation velocities are measured in a distance of 0.5 mm above the test plate. At the position $x = 12$ cm the boundary layer wave breaks up into turbulence. There the exponential increase ends.

With a given flow velocity $U_\infty$ the excitation of boundary layer waves is most effective at a certain frequency $f_c$, the frequency of coincidence. At other frequencies, the boundary layer wave excitation is possible only with strongly increased amplitudes of the plate surface. For each driving system of slits the frequencies of coincidence are linear functions of the flow velocities. The results of measurement are plotted in *Fig. 4*. In addition to the results for the driving system with $\lambda_o = 28$ mm, points corresponding to $\lambda_o/3$ are also shown. These will be discussed below.

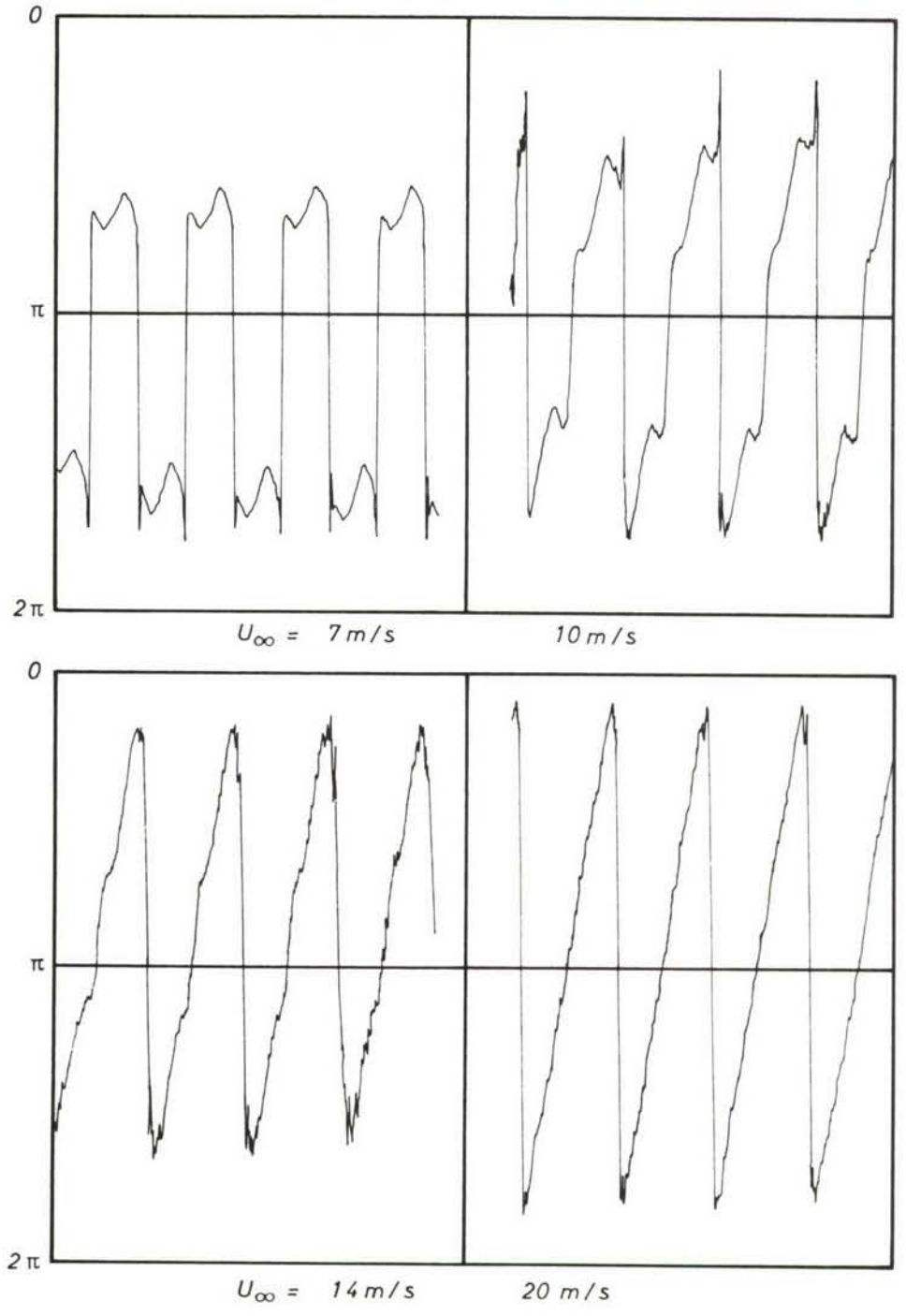


Fig. 2. Phase distribution of the velocity oscillations in the boundary layer along driving system for several flow velocities. $f_s = 543$ cps.

At coincidence the wavelength of the induced boundary layer wave is equal to the double slit distance $\lambda_o$, i.e. equal to the wavelength of the flexural wave of the test plate. The phase velocity $c_r$ of the boundary layer wave therefore increases linearly with the flow velocity $U\infty$ For all driving systems the ratio of the phase velocity and the flow velocity $c_r/U\infty = \lambda_o f/U\infty$ is within the limits of 0.325 and 0.45. A comparison with the theory of stability of the flow along

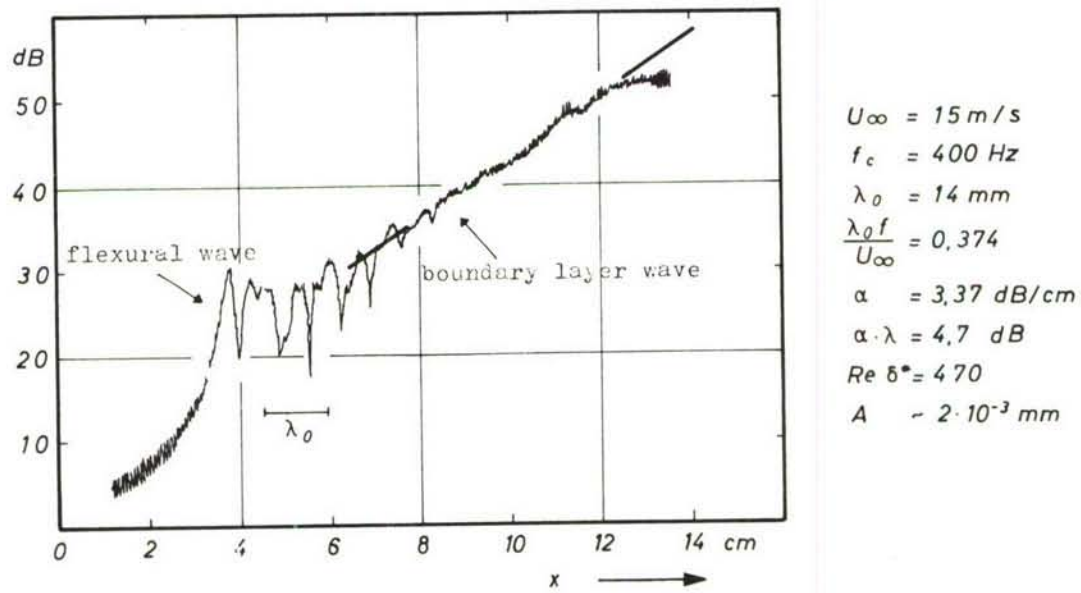


Fig. 3. Excitation of a boundary layer wave by a flexural wave. Ordinate in logarithmic scale.

a plate (ref. 19) indicates that the measured values of $c_r/U\infty$ are in the zone of instable phase velocities. In *Fig.* 5 all measured values and the theoretical curve for indifferent waves are shown. From this it can be seen that the wavelike deformation of the test plate will excitate boundary layer waves if the phase velocity of the deformation is within the range of phase velocities of the instable boundary layer waves.

The stability theory is not only phase velocity dependent but is also frequency dependent. Therefore, only boundary layer waves with certain phase velocities together with certain frequencies are instable. With the present method of excitation the frequency condition becomes less stringent. The coincidence frequencies are not always in the instability range. However, as the coincidence frequencies approach the center of the instability range the deformation amplitude of the plate necessary for boundary layer wave excitation becomes smaller.

## THRESHOLD AMPLITUDES

In order to have a measure for the comparison of the excitation amplitudes a threshold amplitude will be defined. The velocity oscillations in the boundary layer at a fixed position, x, behind the driving system increase very abruptly if these amplitudes exceed a certain value.

The amplitude of the velocity oscillations of the flexural wave at which this increase occurs is defined as the threshold amplitude.

In Fig. 4 we have seen that not only could the boundary layer wave with the wavelength equal to $\lambda_o$=28 mm be excited, but the wave of a wavelength $\lambda_o/3$ was also excited. Principally

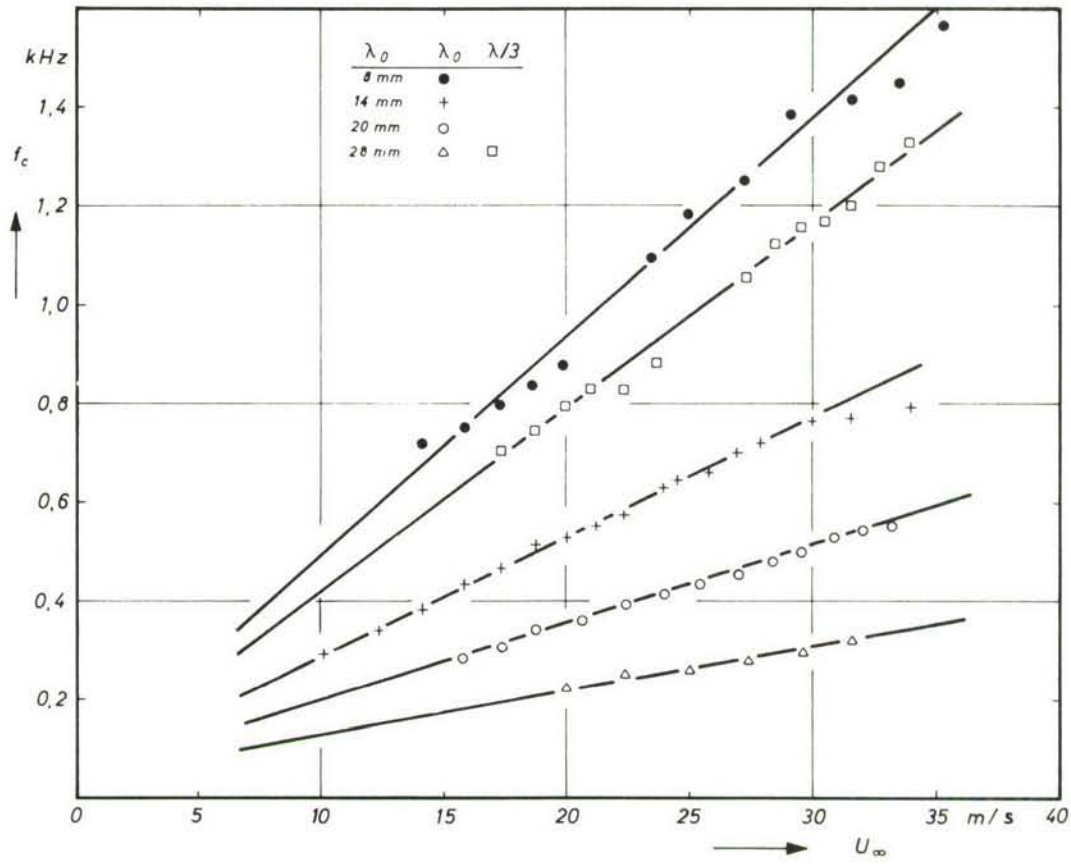


Fig. 4. Coincidence frequencies of the different driving systems as a function of flow velocity.

the excitation of waves with the wavelength equal to an odd fraction of $\lambda_0$ is possible as the flexural wave is sampled only in two points per wavelength. Therefore, coincidence along the entire driving system is possible for these fractions. As can be seen from *Fig. 6* the boundary layer wave with the wavelength $\lambda_0 = 28$ mm is far below the instability range whereas the boundary layer wave with $\lambda_0/3$ is within the instability range. Therefore, the threshold amplitude for the fundamental mode ($\lambda_0$) exceeds that of the second mode ($\lambda_0/3$) by more than 12 dB. The other curves of Fig. 6 represent the coincidence frequencies for the other driving systems. They are both in the interior and in the exterior of the instability range. The ordinate of that figure is the nondimensional frequency $2\pi f\delta^*/U\infty$ which allows a better comparison with the theoretical neutral lines.

The measured threshold amplitudes for the different driving systems cannot be compared in an absolute scale. In *Fig. 7* the threshold amplitudes therefore are normalized to yield the same value for the flow velocity $U\infty = 20$ m/sec. Then all measured values arrange themselves around one curve. The threshold amplitudes decrease strongly with increasing flow velocity. In this representation the phase velocity for all driving systems is the same for a given flow velocity.

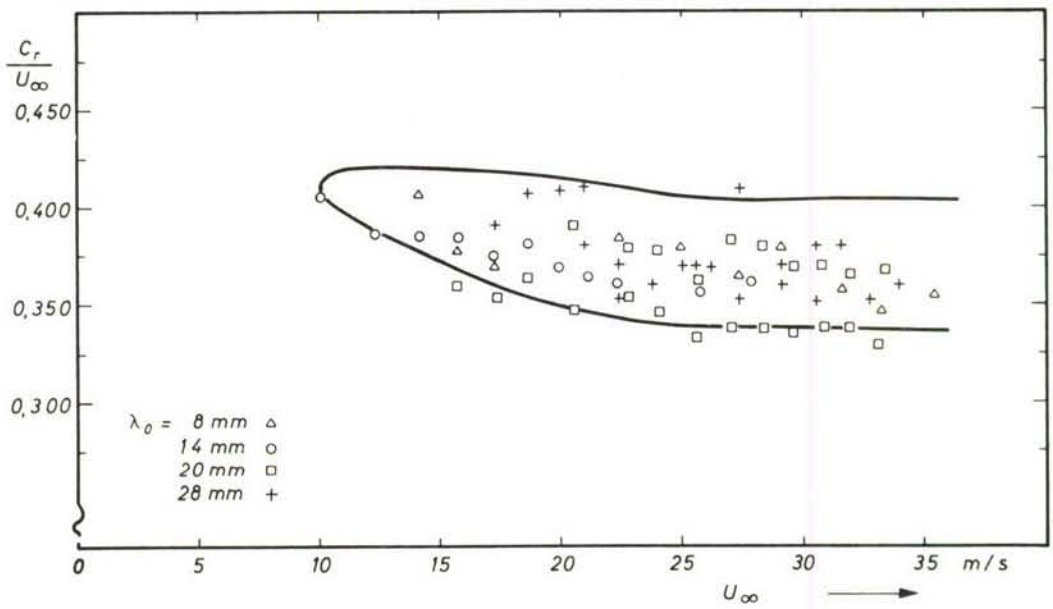


Fig. 5. Comparison of the measured normalized phase velocity with the theoretical instability range.

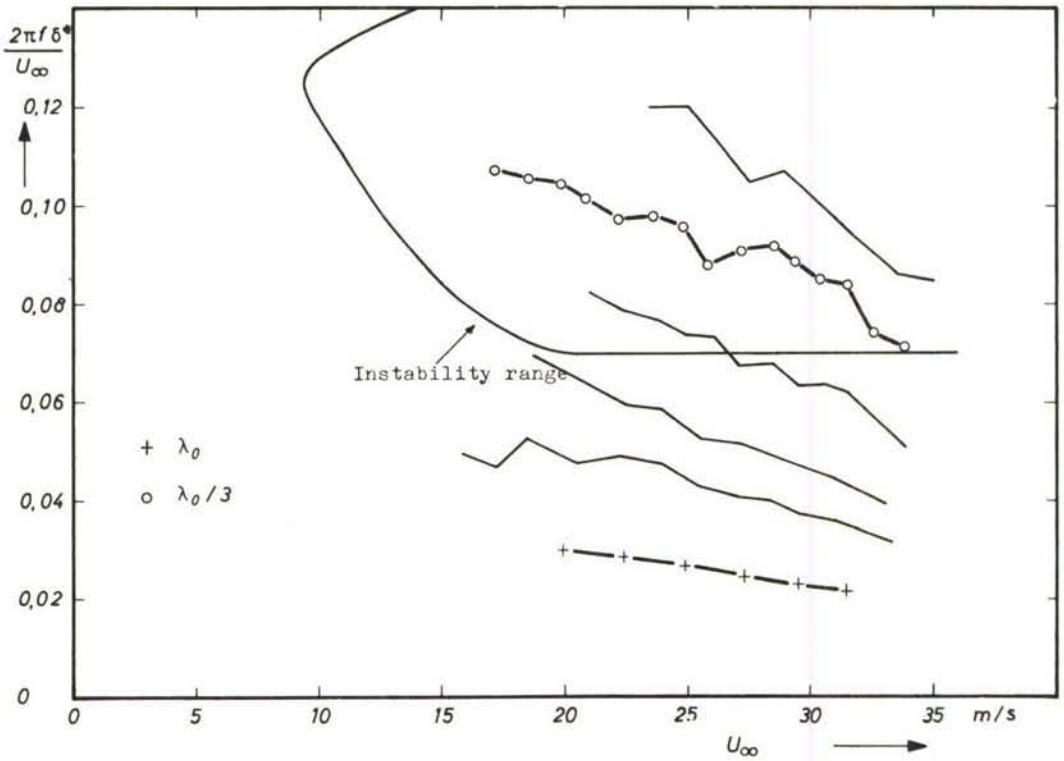


Fig. 6. Comparison of the fundamental mode and of the second mode with the theoretical instability range for the driving system with $\lambda_0 = 28$ mm. (Additional curves for the other driving systems.)

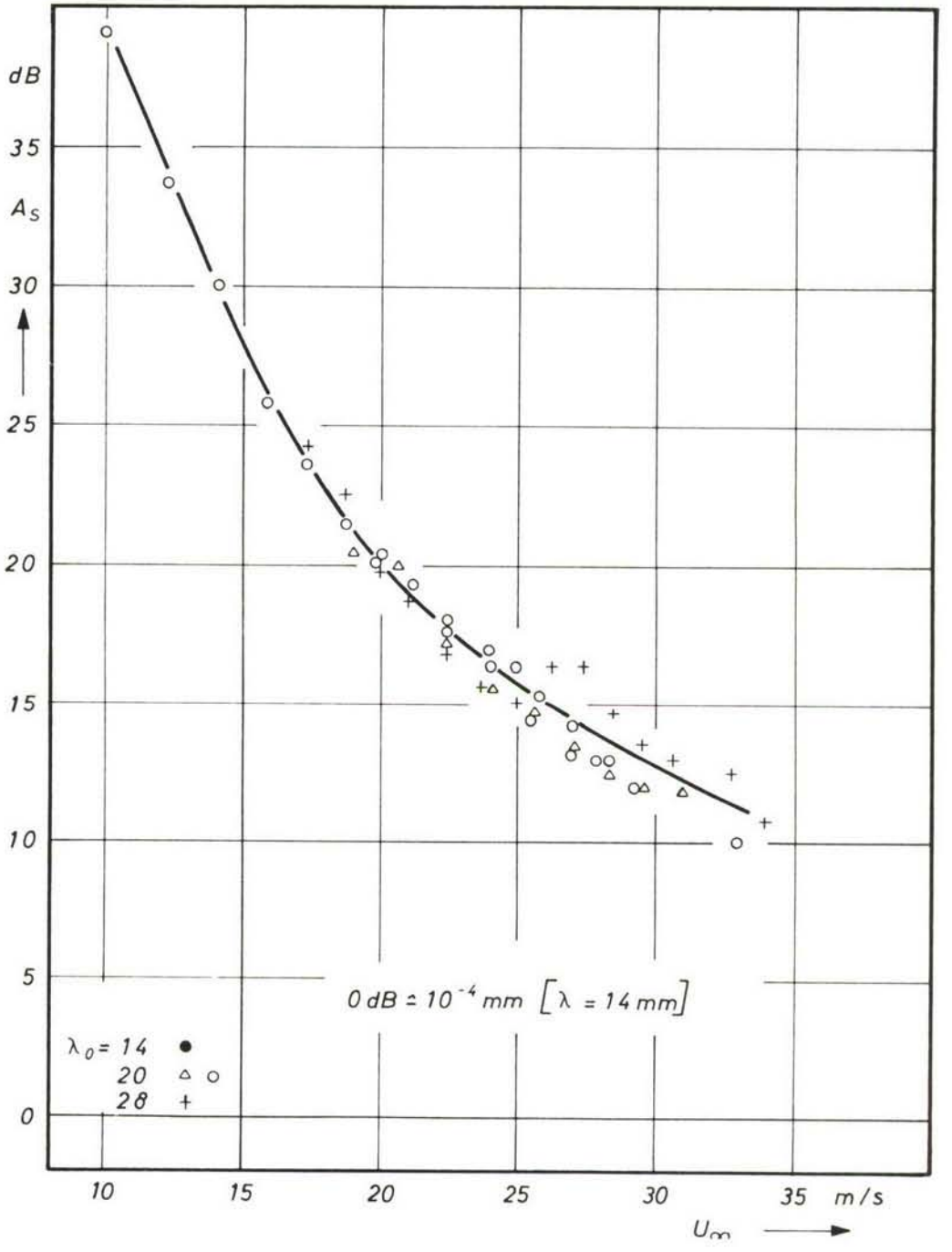


Fig. 7. Relative threshold amplitudes at coincidence vs. flow velocity. Normalized for equal values at $U\infty = 20$ m/sec.

By multiplication of the abscissa values by 0.375 the phase velocity is obtained. The ordinate of Fig. 7 is in a logarithmic scale. The threshold amplitude of the system with $\lambda_o = 14$ mm is $10^{-4}$ mm for the ordinate value 0 dB.

## EXCITATION OF BOUNDARY LAYER WAVES OUT OF COINCIDENCE

The threshold amplitudes and the phase velocities of the induced boundary layer waves were also measured for frequencies different from the coincidence frequency. The results confirm the above statements. The threshold amplitude measured as a function of driving frequency

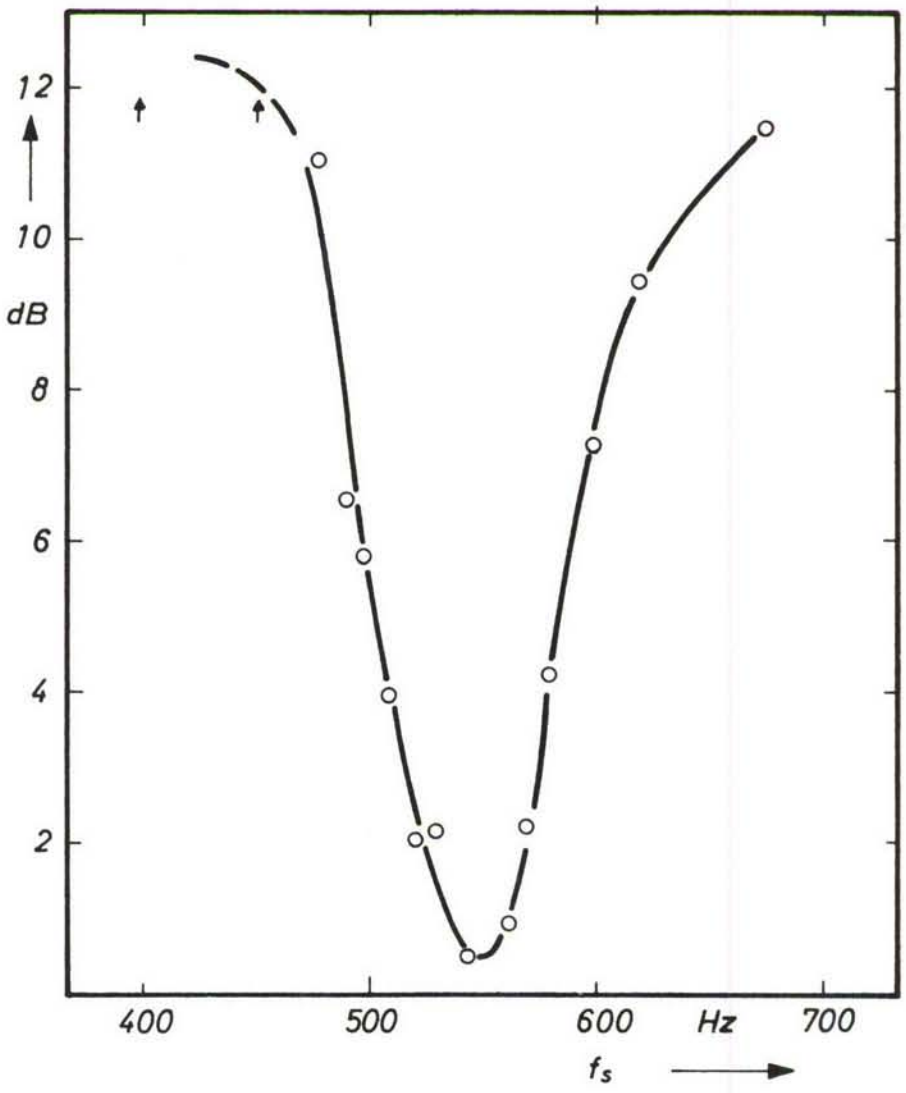


Fig. 8. Threshold amplitudes vs. frequency for constant flow velocity $U\infty = 20$ m/sec.

at the constant flow velocity $U\infty = 20$ m/sec has a marked minimum at coincidence, *Fig. 8*. The coincidence frequency is 543 cps. *Fig. 9* shows the corresponding normalized phase velocity $c_r/U\infty$. The straight line $c_r/U\infty = 0.374$ indicates the center of the instability range. At coincidence the measured curves cross this straight line. For frequencies different from the coincidence frequency the wavelength of the induced boundary layer wave is different from the wavelength of the surface deformation indicated by the straight line $\lambda = 14$ mm. The wavelength of the boundary layer wave is nearer to the instability range. The spatial synchronization by the wall deformation is incomplete. Behind the driving system where the synchronization terminates, the wavelength of the induced boundary layer wave changes so that it falls into the interior of the instability

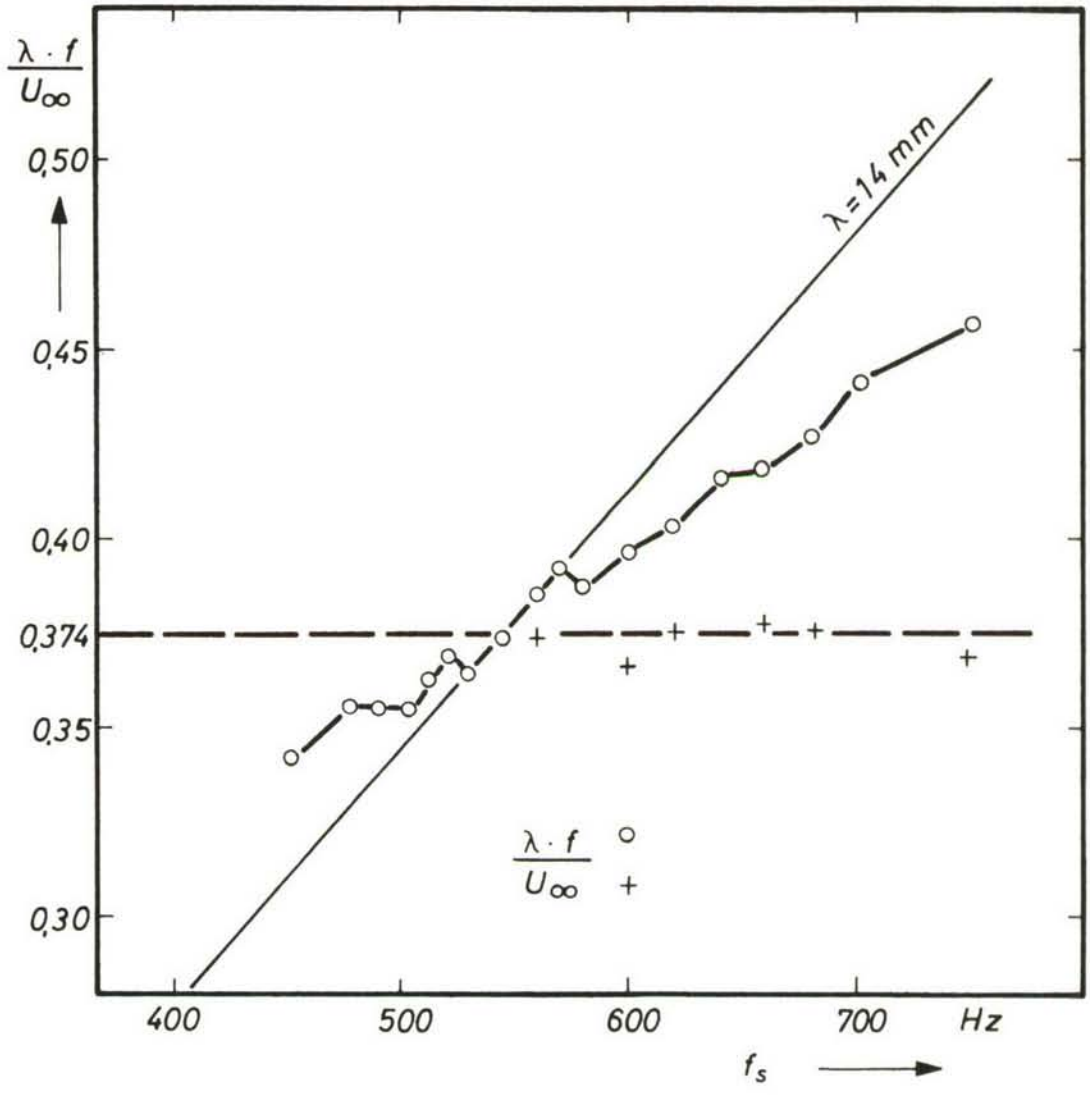


Fig. 9. Phase velocity of the induced boundary layer wave in front of and behind the driving system as a function of frequency for constant flow velocity $U\infty = 20$ m/sec.

range. For some frequencies f higher than $f_c$ the phase velocities in the section of the driving system as well as behind the system are entered into Fig. 9.

For the further investigation of the interaction between a flexural wave and the flow boundary layer an arrangement is planned which will allow a quantitative measurement of the threshold amplitudes at different wavelengths. This arrangement consists of an array of 50 electromagnetic vibrators each 3 mm thick. The amplitudes and phases of each vibrator can be regulated individually. The system has a length of 20 cm. Thus wavelengths between 0.8 and 20 cm can be realized. Furthermore the flexural wave can be sampled by this system with more sampling points per wavelength. The energy flow between driving system and boundary layer shall be measured and compared with the theory (ref. 2).

In other experiments the influence of the induced boundary layer waves on distortions of the boundary layer otherwise generated shall be investigated. Preliminary measurements revealed the possibility to withdraw energy from the boundary layer waves thereby reducing boundary layer distortions.

## SECTION III.

# Sound Propagation In Ducts with Superimposed Air Flow

## PROPAGATION OF PRESSURE PULSES IN A FLOW DUCT

### Introduction

Until now it was impossible to generate a plane sound field in a duct with sound wave lengths of the order of the aerodynamical boundary layer thickness and to measure its alteration by a turbulent flow profile. This situation was corrected by generating a short pressure pulse in the duct by means of a spark discharge. Thus a defined spherical wave front is achieved which propagates with sound velocity within the duct. The way in which a wave front will be altered by the flow superposition and the statements which can be made about the transport of sound energy are reported.

### Experimental Set-Up

For this purpose a $4\mu$F condenser is loaded with 4 Kilovolts and is discharged through a spark plug. The spark plug is inserted into the bottom of the duct midway between the duct walls. The thickness of the positive pressure phase of the wave front measured by a condenser microphone is smaller than 0.14 cm. With normal sound velocity the equivalent frequency is approximately 60 kcps. From propagation time measurements, the sound velocity came out to be 344 m/sec under normal conditions.

The shape of the wave front was first determined from propagation time measurements by checking the sound field point by point with a microphone. However, the accuracy achieved was insufficient because of unequal spark discharges and the finite size of the microphone. Therefore, a schlieren method is applied for determining the wave shapes.

The image forming concave mirror lenses of the schlieren apparatus have a focal length of 150 cm and a diameter of 15 cm. The field of observation in the plane of the axis of the duct is 10 x 10 cm$^2$. *Fig. 10* gives a schematic view of the set-up.

By pressure gradients in the plane of observation, the parallel light is diffracted and is more or less masked by the schlieren edge. For the detection of the pressure front which travels with sound velocity, the entrance slit is illuminated by an electric spark. Its duration is less than 0.5 $\mu$sec. Thus a standing picture of the wave front can be taken. The illuminating spark is triggered after an adjustable delay time by the spark discharge. The delay time is chosen according to the travelling time of the sound pulse from the spark plug to the observation windows in the duct walls.

In the flow velocity range from 0 to 100 m/sec used here, the flow can be considered nearly incompressible. Thus no appreciable pressure gradients will be generated by the turbulent flow itself. Experiments proved that with the sensitivity of the above set-up no schlieren of the flow can be observed, and that up to high flow velocities the wave front of a pressure pulse was still visible.

Since the pressure pulse propagates as a spherical wave, its amplitude is geometrically attenuated. However, after a travelling-path of at least 60 cm in the rigid duct the amplitude of the pressure pulse is sufficiently high to give schlieren pictures of the wave front. Greater distances have not yet been examined.

## Experimental Results

The wave fronts of the pressure pulse were photographed with the apparatus described above. The travelling-path of the pressure pulse was altered by displacements of the spark plug

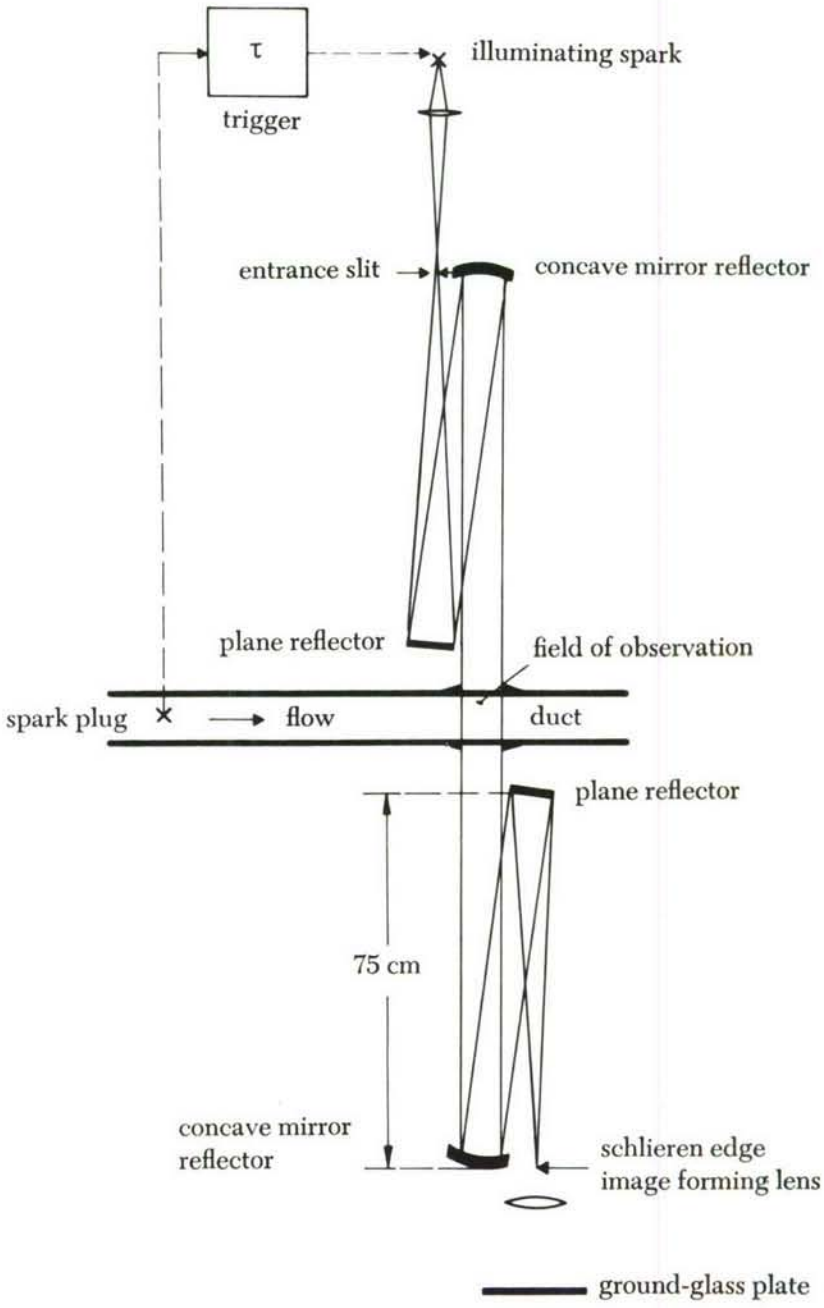


Fig. 10. Schematical view of the schlieren apparatus.

along the bottom of the duct. The boundary layer thickness was increased artificially by inserting a fence made of four parallel wires of 2 mm diameter each at the entrance of the measuring section of the duct. Without this fence the boundary layer thickness would be about 5 mm. In *Fig. 11* the measured flow velocity profiles are shown for several distances from the fence. The fence increases the turbulence level, too. The measurements yield velocity profiles which rise from about 20 m/sec near the wall to about 30 m/sec in a distance of 6 cm from the wall and then remain constant. The rise is nearly linear. Since the shape of the profile changes but little with the axial distance from the fence, the sound propagates in an inhomogeneous medium with a constant gradient.

The schlieren photographs of the pressure pulse are shown in *Fig. 12*. The wave fronts for sound propagation without flow are in the first row. Parameter within the row is the distance of the spark plug from the position where the wave front touches the bottom of the duct. The pictures are typical for a spherical wave front propagating in a square duct. The reflections from the rigid walls of the duct become visible as wave fronts lagging behind the first wave front. The first wave front is perpendicular to the bottom of the duct.

The second row contains the pictures of the wave front with the flow described above superimposed. From these it can be seen that the angle between the first wave front and the bottom of the duct is smaller than 90° with the wave front inclined in the direction of the flow. From the inclination of the front it can be concluded that the propagation of the sound energy near the wall is directed towards the latter. The distinction of the branches are reflected specularly

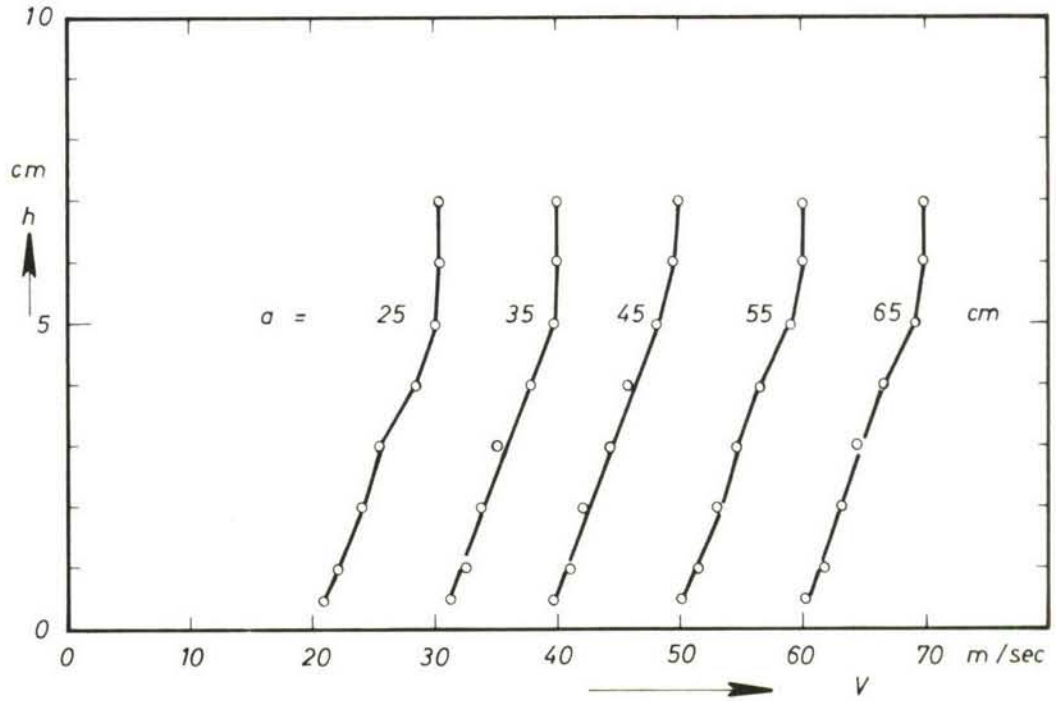


Fig. 11. Flow velocity profiles for several distances $a$ from fence. (Profiles are shifted for 10 m/sec each, except first one.)

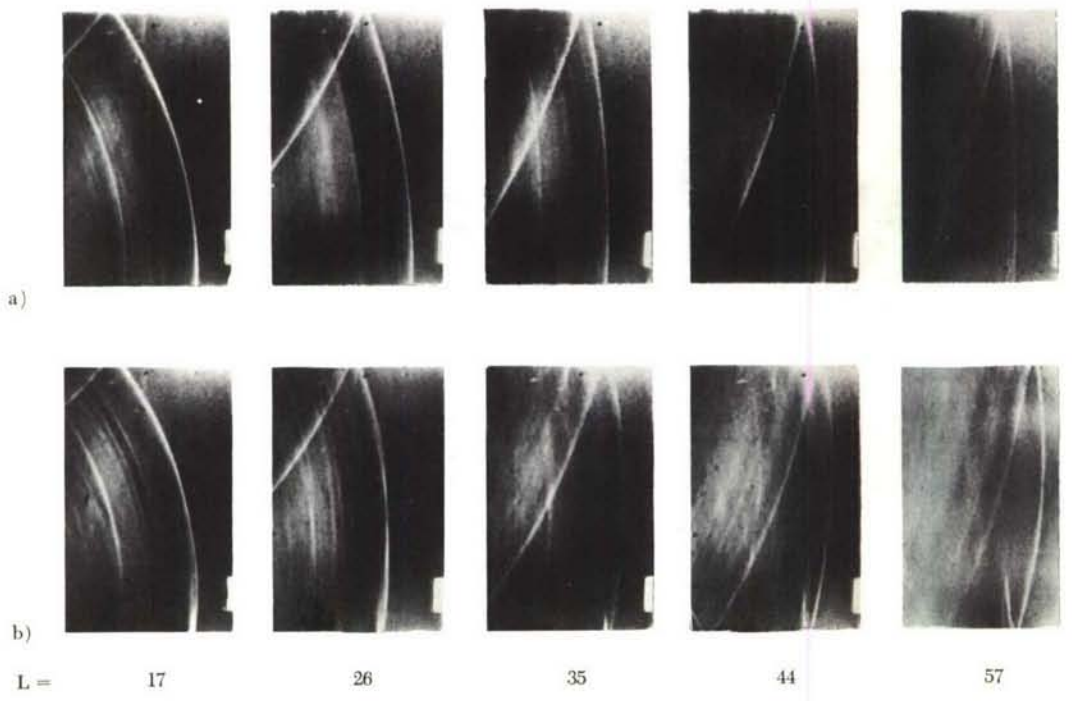


Fig. 12. First wave front as a function of length of travelling-path L
a. without flow
b. with flow according to Fig. 11

from the ground-contact point of the wave front backwards into the duct directly proportional to the travel-path length. Their length increases with the travelling-path. In greater distances from the wall these branches are no longer specular to the first wave front. They are inclined in the flow direction. The appearance of these branches is caused by the gradient of the flow velocity near the wall. As the wave front is inclined towards the wall continuous reflection takes place.

In a further set of measurements the rigid bottom of the wall was replaced by a Rayleigh absorber made of corrugated paper. Its average pore width is about 2 mm. Towards the flow the absorber is covered by a porous foil with a resistance of 0.25 $\rho c_0$. On the rear side the absorber is terminated by a rigid wall. The flow profiles remained the same as before. The wave fronts with this arrangement are shown in *Fig. 13*. By comparison with Fig. 12b, it follows that the first wave fronts coincide for equal lengths of the travelling-path. The reflected branches, however, are suppressed. The absorber is well matched to the characteristic impedence of the duct. Therefore, the acoustic energy contained otherwise in the branches is absorbed. Compared with the no-flow condition the sound absorption is increased by the gradient of the flow velocity. The shape of the wave fronts without flow is the same with the absorber and the rigid wall respectively. The magnitude of the sound absorption could not yet be determined. It cannot be very high, however, since the wave front without flow remains visible near the absorber even for long travelling-paths.

From the present results it can be expected that the reflected branch of the wave front, on its further path, will be directed towards the wall just as the first wave front, and there, will produce another reflected branch. This branch will lag behind the first wave front as the first branch which generates it has to go through zones of smaller flow velocities. Thus the wave front is split into many branches. The wave front undergoes a spatial dispersion.

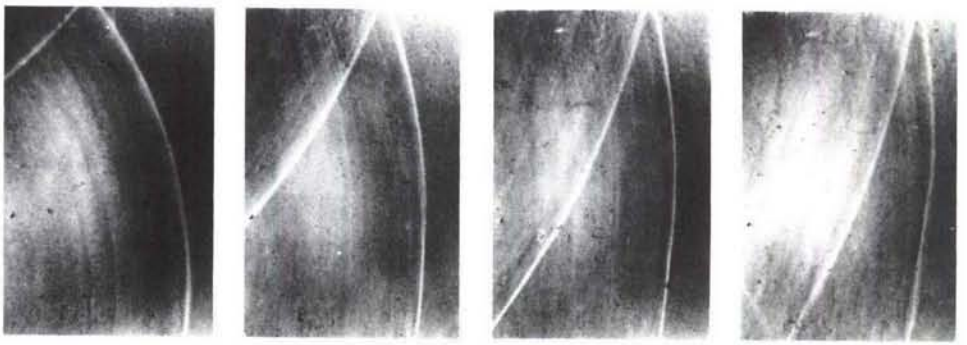


Fig. 13. First wave front for several lengths of travelling-path L along sound absorber, with flow.

## Interpretation by Geometrical Acoustics

It was shown by Heller (ref. 5) that the eikonal equation holds for the wave fronts of weak pressure pulses. For the problem at hand it is:

$$|\nabla\Phi| = c_o/(c_o + \vec{V} \cdot \nabla\Phi / |\Phi|).$$

Here $c_o$ is the sound velocity, $\vec{V}$ the flow velocity and $\Phi$ is the function of the wave front. From this Kornhauser (ref. 9) deduces a differential equation for the acoustic rays in a stratified medium:

$$\frac{dy}{dx} = \frac{\sqrt{1 - 2MC - C^2(1-M^2)}}{M + C(1-M^2)} \qquad (1)$$

where x is the direction of the flow, $M = M(y)$ the Mach number which is a function of the distance from the wall at $y = O$ with $M(O) = O$ and C is a parameter which is constant for a given ray. C is the cosine of the glance angle of the ray at the wall. For a flow with constant flow velocity, $M = \text{const.}$, eq. (1) yields straight lines. With a variable flow velocity the rays have their greatest distance from the wall where the numerator of the right side of eq. (1) vanishes. In this case $M = (1 - C)/C$. If M is an unique function of y a ray with a given glance angle can reach only a certain maximum height above the bottom of the duct. From there on it is directed again towards the bottom. The distance from the sound source at which it again touches the bottom depends on the details of the function $M(y)$.

From eq. (1) the sound rays were computed for a flow velocity profile with a linear increase from 20 m/sec near the wall to 30 m/sec at 6 cm from the wall. They are represented in *Fig. 14*. Parameter of the rays is the maximum height. The first wave front taken from the

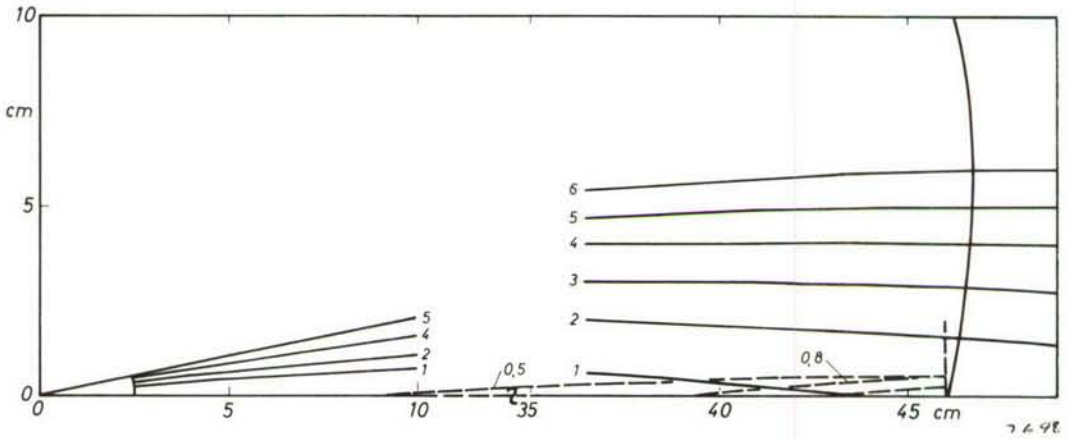


Fig. 14. Computed sound rays. Parameter: Maximum distance from wall in centimeters.

measurements are also shown in *Fig. 14*. In general (ref. 9) the normal of the wave front does not coincide with the direction of the ray. In the present measurements, however, the directions are only a little different from each other as the glance angles are small and the flow velocity is much less than the sound velocity. The rays in Fig. 14 represented by broken lines have been reflected once at the wall. They correspond to the dashed reflected branch of the wave front. The maximum height of the reflected ray is about 0.5 cm at the position of the plotted wave front. All rays which have been reflected between this position and the sound source remain below this height. It is true, however, that the reflected branch observed in the measurements extends to a greater wall distance. This may be caused by scattering of sound which is neglected in the theory of geometrical acoustics.

With the described flow distribution used in the present measurements all rays with a glance angle smaller than 23 degrees remain within the flow boundary layer of 6 cm thickness. Thus the boundary layer represents a wave guide (see for example ref. 4). The sound energy contained in the guide is conserved if there are no losses by scattering. With a shock wave, however, the front can undergo spatial dispersion. All rays with greater glance angles reach the zone of constant flow velocity above the boundary layer with a non-zero angle. There they propagate along straight lines until they penetrate into the upper boundary layer and are reflected at the upper wall.

## NONLINEARITY OF SOUND ABSORBERS WITH SUPERIMPOSED AIR FLOW

### Measurement of the Absorber Impedance with Grazing Flow

For testing the influence of flow on the acoustic input impedance of absorbers a Kundt's tube was used which allowed the impedance to be measured under flow conditions. For this purpose the tube was fastened perpendicular to the flow duct so that its front end matched with the duct wall. The absorber is inserted into the tube with its surface being even with the duct wall. Then for not too thick absorbing layers the input impedance of the surface can be determined from

behind by the standing wave ratio and the position of the pressure nodes. The impedance measured from behind is a series connection of the absorber impedance and the resistance of the two connected duct branches. This last part must be measured separately without absorber and be subtracted from the impedance determined with absorber. Care had been taken to prevent air flowing through the absorbing material by tightening the tube. The tube diameter is 7 cm.

As objects to be measured were chosen: a rockwool layer ("Sillan") of 1 cm thickness, a porous foil and a 0.5 mm thick resilient plate ("Pertinax") which was glued at the brim. *Fig. 15* shows the real and imaginary impedance at 0 and 40 m/sec flow velocity for the porous materials subjected to frequencies between 1.0 and 1.6 kc and for the flat plate subjected to frequencies between 0.6 and 0.8 kc. The real part of the impedance without absorber is drawn into the diagram for the rockwool absorber. Here the front of the tube was covered with a gauze screen to provide better flow guidance. Its acoustic resistance is negligible.

As can be seen from the pictures none of the samples shows a marked influence of the flow. The deviations lie within the measuring accuracy. For porous materials they amount to less than 10 per cent on the average. According to the results in (ref. 18) the real part of the impedance of the rockwool layer should have been increased by about 35 per cent by alteration of the inner flow resistance. Also the plate resonator does not show an effect of the flow even in the resonance region. In connection with these measurements the turbulence level in the duct was enlarged by the insertion of turbulence grids and the Kundt's tube was opened at its rear end to allow the air flowing through the absorber. However, an alteration of the flow resistance was not found.

According to these results it seems unlikely that under the given circumstances the absorber becomes nonlinear thus altering its effective input impedance.

## Measurement of the Absorber Impedance with Penetrating Flow

As porous absorbers are known to become nonlinear when exposed to vigorous sound fields (high particle velocities) this report shall show the behavior of such absorbers when there is a constant flow through them.

For this purpose the impedance of porous absorbers was measured. The set-up is schematically drawn in Fig. 16. It consists of a Kundt's tube in the middle of which the absorber to be tested can be inserted. The tube section at the rear end of the sample is terminated reflectionless by a 30 cm long wedge of rockwool. As this wedge does not fill up the entire cross-section of the tube air can be sucked through the tube by a blower at this end. The tube has a free diameter of 7 cm and the maximum flow velocity without insertion of a sample appeared to be about 5 m/sec. Without any sample inserted the standing wave ratio in the front part of the tube amounted 0.95 to 1.0 in the frequency range between 1.0 and 2.0 kc. With that the acoustic load at the rear end of the absorbing sample is $(1.0 \pm 0.05)\ \rho c_0$.

The difference of the static pressures between front and rear end of the sample can be measured with a pressure gauge. A hot-wire anemometer is applied to determine the flow velocity. The hot-wire is calibrated vs. a Pitot tube at low flow velocities. The position of the hot-wire is about 15 cm downstream from the open end of the tube and in the center. The mean flow velocity is 0.85 times the center velocity. (This value was attained by checking the flow profile across the cross-section of the tube.)

The impedances of a 1 mm thick porous foil and a 1 cm thick rockwool layer were determined from the standing wave ratio and the position of the pressure nodes at different flow velocities. Since low flow velocities were used, corrections due to an alteration of the acoustic wave length could be neglected. In the above mentioned frequency range the thickness of the samples is small

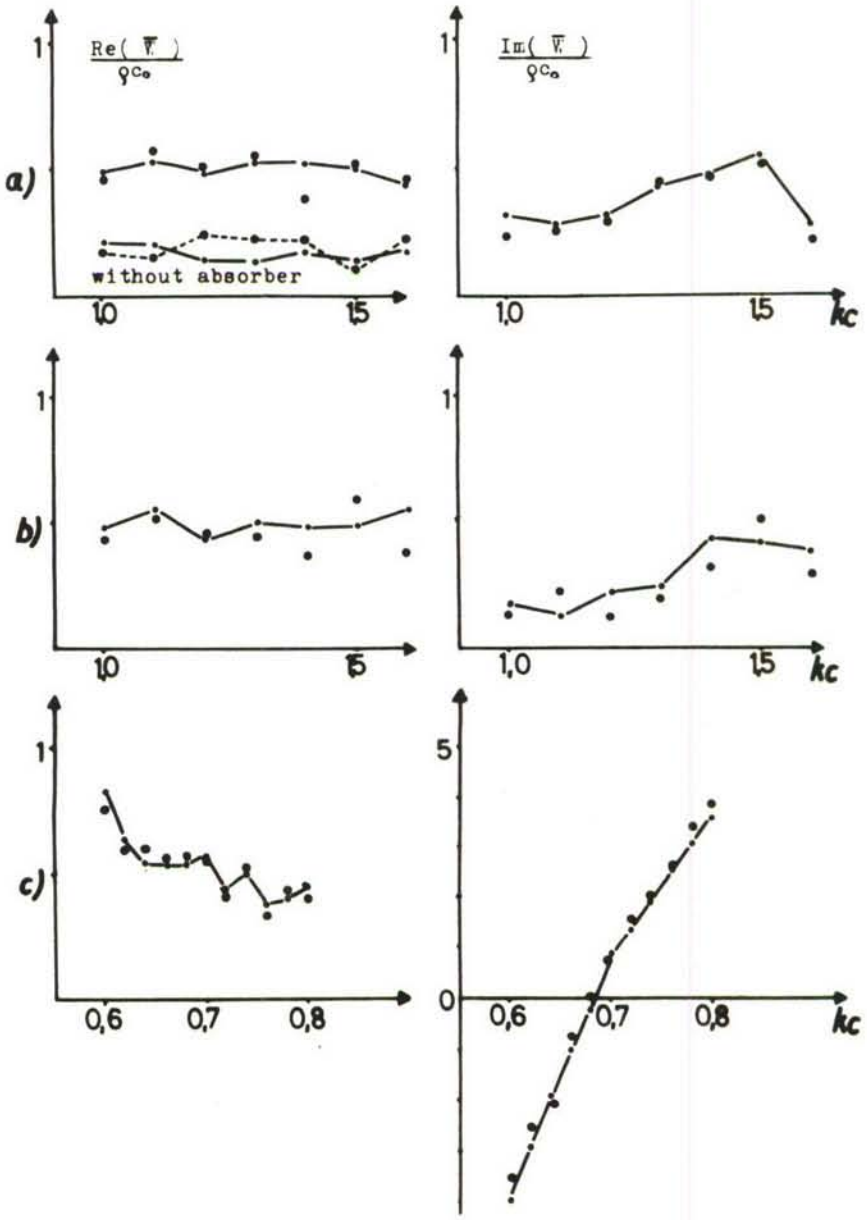


Fig. 15. Real and imaginary parts of the impedance at (·) 0 m/sec and at (o) 40 m/sec flow velocity
a. of a 1 cm thick rockwool layer
b. of a porous foil
c. of a resilient plate

compared to the wave length so that after subtraction of the rear load of the sample the impedance yields directly the acoustic flow resistance. The measuring accuracy of the acoustically attained impedance values is about 0.1 $\rho c_0$.

In order to prevent the absorber becoming non-linear by excessively high sound amplitudes, the particle velocity was held below 1 cm/sec. Up to this value no sign of non-linearity could be observed at resting air.

The impedance measurements were mainly made at a frequency of 1.0 kc because a remarkable frequency dependency was not found between 1.0 and 2.0 kc.

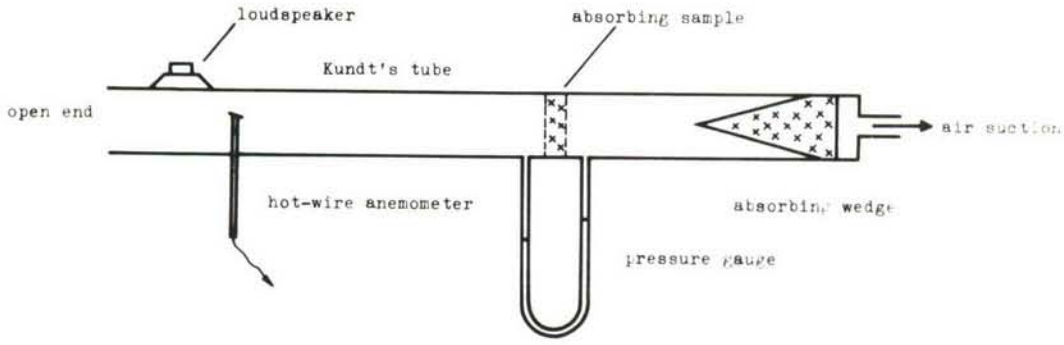


Fig. 16. Schematic set-up for impedance measurements of porous absorbers.

In *Fig. 17 and 18* the acoustic flow resistances of the different samples are plotted vs. the flow velocity. As can be seen both materials show a linear increase of the flow resistance starting from the value at resting air. The flow resistance $r_v$ can be represented as a function the flow velocity V by the formula:

$$\frac{r_v}{r_o} = 1 + A_v \cdot V$$

with $r_o$ being the resistance at resting air and $A_v$ a material dependent constant. $A_v$ can be taken as a measure of the non-linearity of the material. It amounts 1.05 sec/m for the porous foil and 0.42 sec/m for rockwool ("Sillan").

In the same figures the static pressure differences vs. the flow velocity are entered. From the resulting curves a more than linear ascent of the pressure with increasing flow velocity can be discerned. From these the differential flow resistance was calculated by numerical differentiation and the received values were entered in the diagrams of the acoustically measured resistance. The statically obtained values are found to scatter with an accuracy of about 20 per cent around the acoustically achieved straight line. With respect to the error faculties of the numerical differentiation the agreement can be considered sufficient. Thus the measurements yield an equivalence of the acoustically found flow resistance and the statical differential flow resistance. It would be interesting to investigate which structure property determines the amount of the non-linearity coefficient. Since taking a sample of two porous foils yielded the same value of $A_v$, it seems obvious that the non-linearity depends on the structure of the volume and not on the structure of the surface.

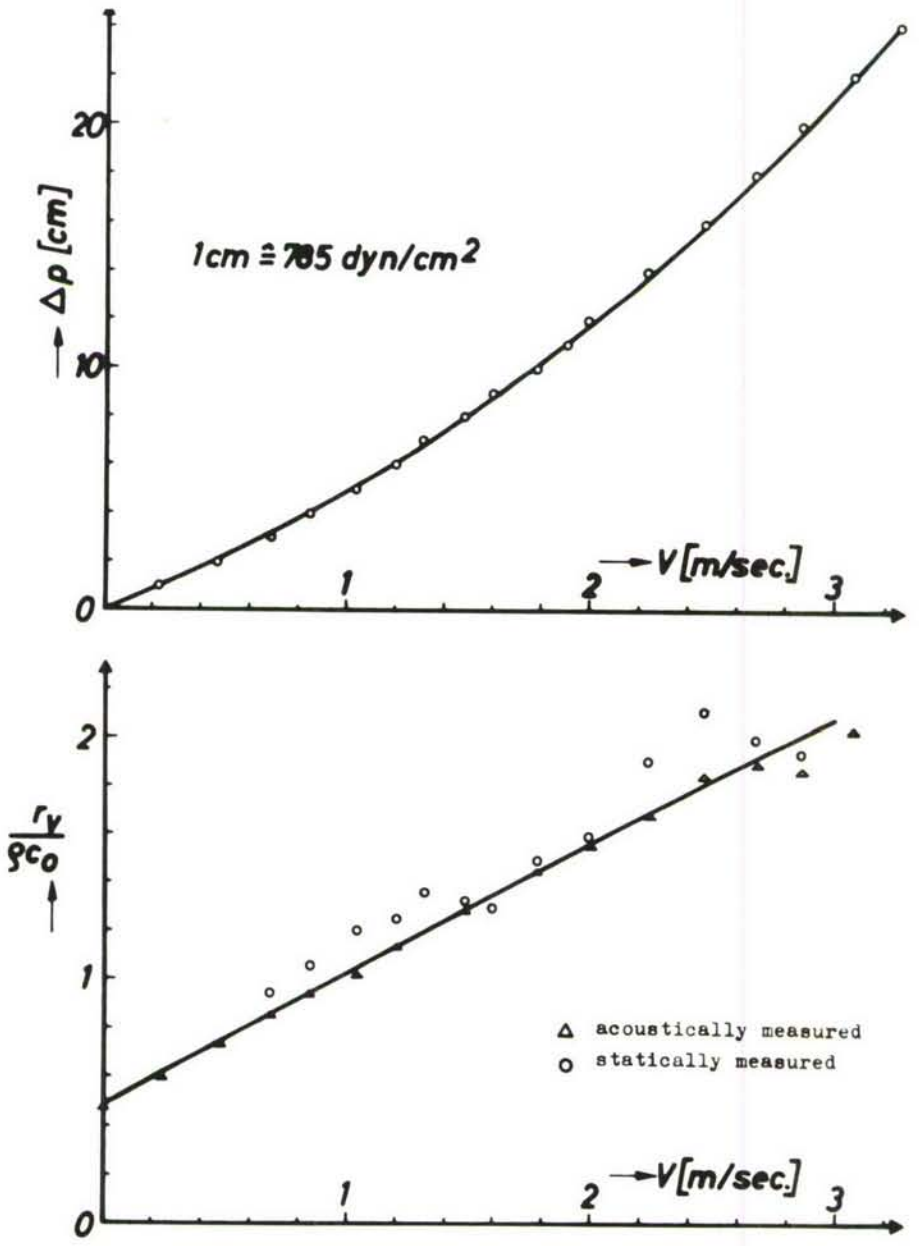


Fig. 17. Difference of the static pressure and flow resistance of a porous foil as a function of the flow velocity.

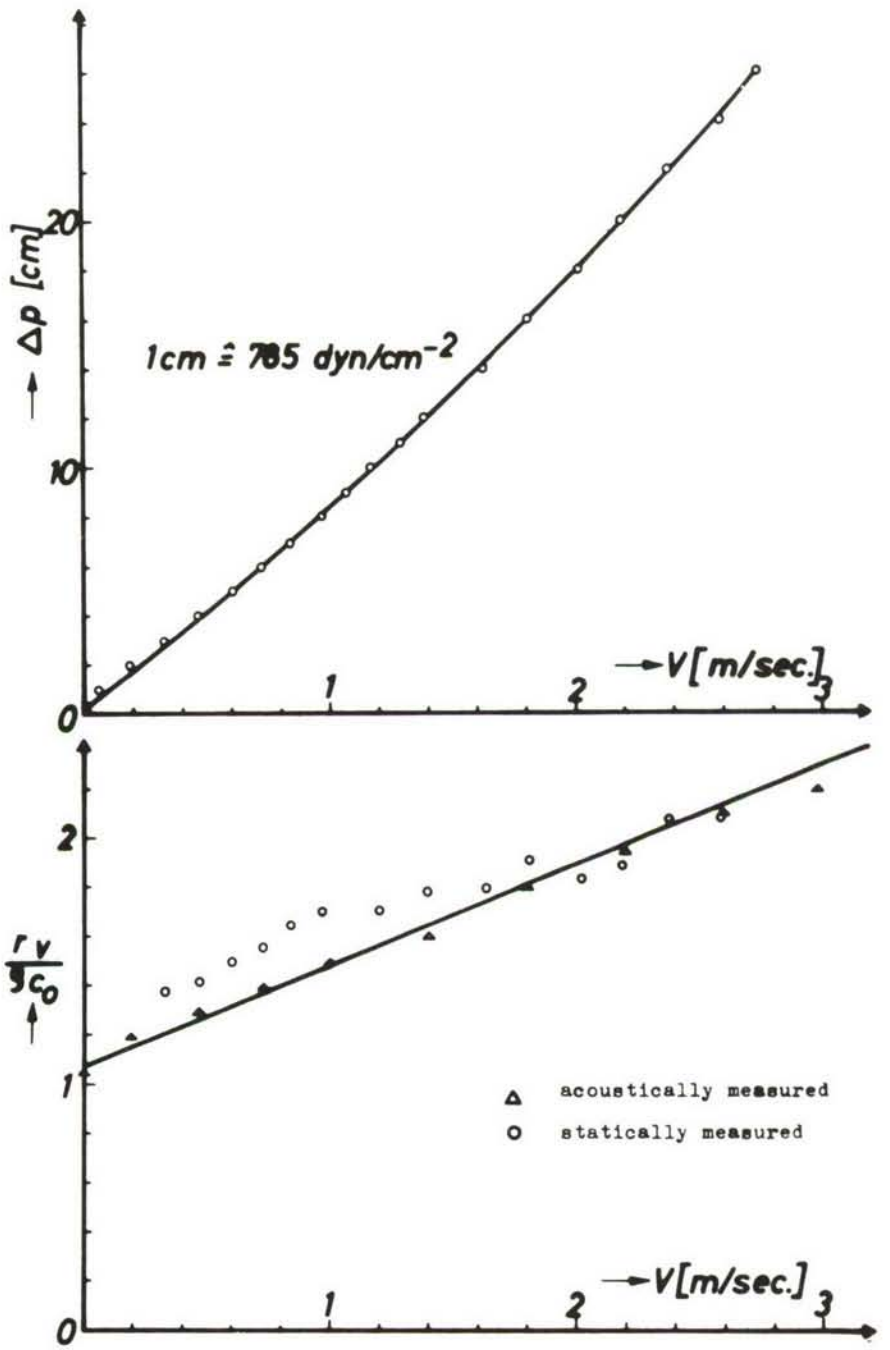


Fig. 18. Difference of the static pressure and flow resistance of a 1 cm thick rockwool layer as a function of the flow velocity.

## SECTION IV.

# Orifice Radiation Impedance as a Function of Flow

## INTRODUCTION

The radiation of sound propagating in a tube through the orifice is determined by the reflection coefficient of the tube termination or by its radiation impedance. Thus, there is an increase in the amount of sound radiated as the reflection coefficient decreases or as the radiation impedance approaches the acoustic impedance of free space. Since the tube is terminated by the radiation impedance of the orifice in the sense of the transmission theory, a change of the radiation impedance will influence the resonances of the tube if any.

### Existing Papers

The determination of the radiation impedance of tube orifices without stationary flow can be said to be a solved problem. Only few papers exist, however, which have some relation to the sound radiation of orifices with flow discharge. Lutz (ref. 11) tries to cover the problem by a very simplified theoretical relation between the acoustic resistance of a diaphragm at the orifice of a tube with stationary flow and the static pressure drop at the diaphragm. In refs. 1, 7, and 24) some measurements are reported with diaphragms with one or more apertures in a tube with stationary flow. The acoustic resistance of these diaphragms is found to increase linearly with the flow velocity. This increase again is ascribed to the static pressure drop. Martin (ref. 12) measured the attenuation of acoustic resonances of tube sections with flow at low frequencies.

According to measurements reported in (ref. 7) the reactance of diaphragms is decreased by the air flow. According to theoretical results by Westervelt (refs. 25, 26) the acoustic impedance of a circular aperture in a thin diaphragm with a diameter of the aperture much smaller than the wavelength can be decreased as much as 40 per cent by the onset of turbulent flows at the diaphragm. Ingard's measurements in (ref. 8) affirmed this statement.

### Scope of this Paper

In this paper measurements of the acoustic reflection coefficient and of the acoustic radiation impedance of circular tube orifices with flow discharge shall be reported. The flow velocity in the tube will range up to 230 m/sec.

Only few results of the cited papers can be applied to the present measurements. At the outlet of a tube without reduction of the cross-section like it is used in these measurements there is no distinct drop of the static pressure as it was true with (refs. 1, 7, 24). The values of $k_o a$ (see List of Symbols) in (ref. 12) are below the range of the present measurements.

By experimental variation of some of the flow parameters the importance of these parameters with respect to the sound radiation shall be investigated.

## MEASURING METHODS

### Flow Generation, Kundt's Tube, Probe Microphone, Measurement of Flow Velocity

The measurements are performed with the wind tunnel described in (ref. 14). The flow generated in a five-stage centrifugal blower (60 kw) is cooled by a water cooler to the constant temperature of 17.5° centigrade in the measuring tube. The sound velocity in the air at rest, therefore, is always 341.5 m/sec. The cooler is followed by a silencer and then by a flow-smoothing section of the duct thereby giving only a small turbulence level in the test section.

An acoustic signal from a 200 watt pressure chamber sound generator is fed into the measuring tube at the tube's most upstream positon. The dimensions of the cylindrical metal tubes used as test sections are given in *Table I*. The radiation is measured at the outlet orifice of the tube. The discharge orifice can be inserted into a baffle of 1.85 x 2 $m^2$ lateral dimensions.

TABLE I.

*Test Section Dimensions and Maximum Flow Velocity*

| Tube Nr. | Inner Diameter | Wall Thickness | Tube Length | Maximum Flow Velocity |
|---|---|---|---|---|
| 1 | 64 mm | 3 mm | 2 mm | 230 m/sec |
| 2 | 85 mm | 5 mm | 2 mm | 180 m/sec |
| 3 | 125 mm | 4 mm | 2 mm | 85 m/sec |

An impedance measuring tube, called a Kundt's tube, proved to be best suited for measurement of the radiation impedance. The standing wave within the measuring tube is picked up by a microphone probe along the tube thus increasing the accuracy of the measurements by averaging along the tube. The sound attenuation in the tube is eliminated by extrapolation to the end of the tube.

The microphone probe is inserted into the tube through the radiating orifice. It moves along the tube axis. Its influence on the sound field in the tube can be neglected (ref. 10) since the probe cross-section is smaller than 1 per cent of the tube cross-section.

The microphone output is filtered with a variable filter of a bandwidth of 10 cps. The sound pressure along the duct was recorded with a level recorder. The linearity of the measuring instruments was checked at several signal amplitudes.

The frequency range of the measurements is limited at low frequencies by the length of the measuring tube of 2.0 meters (frequency limit about 200 cps) and at high frequencies by the onset of higher modes at about $k_o a = 1.8$ (a=inner radius of tube).

The flow velocity in the tube is measured by a Pitot probe on the axis of the tube near the outlet.

The mean flow velocity and the turbulence level in the jet behind the orifice are measured with a hot-wire anemometer which is checked against the Pitot probe within the tube. These measurements, however, are limited to velocities below about 80 m/sec in order to prevent the damage of the probe wires.

## Signal-to-Noise Ratio

The available flow velocities in the tube were limited by the signal-to-noise ratio of the measuring equipment. At the maximum velocities used the signal-to-noise ratio in the pressure antinodes in the tube was about 40 dB for most frequencies. The cross-talk through the walls of the probe (2 to 3 meters in length) was at least 40 dB below the signal through the small sound pick-up borings in the probe wall near the probe tip.

## Influence of Room Reflections

The influence of the reflections from the measuring room on the frenquency response of the sound radiation from the tube was checked by the measurement of the sound field without

flow behind the tube orifice in the baffle. These measurements always yielded a smooth and monotonic decrease of the sound pressure with increasing distance from the orifice. Furthermore, the comparison of the measuring results without flow with the theoretical curves yielded good agreement. Finally, there was no increase in the measuring accuracy when the measurements without flow were repeated in an anechoic chamber.

### Flow in the Measuring Tube

The flow velocity profile within the tube was measured for the tube with the diameter of $2a=85$ mm at flow velocities on the tube axis of $V_{ax}=40$; 80; 120 and 156 m/sec. The flow velocity was found to be constant from the center of the tube until about a/3. Then it decreased towards the wall. By integration of the flow velocity profile the average flow velocity $\overline{V}$ was evaluated. For all flow velocities the relation to the axial flow velocity $V_{ax}$ was

$$\overline{V}=0.87\ V_{ax} \tag{1}$$

From the general law of flow velocities of a turbulent flow in circular tubes (ref. 20) for a Reynolds number of $10^6$, typical for the present measurements, the relation

$$\overline{V}=0.84\ V_{ax} \tag{2}$$

is found. The factor in eq. (2) remains virtually constant for all tubes used in our measurements.

The turbulence level in the orifice is about 1 per cent in the center. It increases towards the walls. In a distance of 5 mm from the wall 7 per cent were measured.

## FOUNDATION OF THE IMPEDANCE MEASUREMENT IN FLOW

### Wave Equation and Impedance Formula

For the evaluation of the reflection coefficient and of the radiation impedance of the tube termination with flow a revision of the well-known formula from the transmission theory is necessary. As a satisfactory approach to the real facts we assume a flow in the tube constant in time and in the lateral extensions. A sound signal is fed into the tube at its one end propagating as a plane wave without losses towards the radiating orifice. At the radiating orifice a partial reflection takes place. Let the coordinate in the direction of the tube be x; the radiating orifice be at $x=0$, and the tube be at negative values of x. The acoustic impedance of the orifice at $x=0$ shall be evaluated from the standing wave in the tube. (The influence of attenuation and of a curved flow velocity profile will be discussed below.)

The total velocity $\underline{v}$ is the sum of the acoustic particle velocity v and the mean flow velocity V:

$$v = \underline{v} + V.$$

From the equation of Newton

$$\rho \frac{dv}{dt} = -\operatorname{grad} p$$

and the equation of continuity

$$\operatorname{div} (\rho v) = -\frac{\partial \rho}{\partial t}$$

together with the adiabatic equation

$$dp = c_o^2 d\rho$$

neglecting all nonlinear acoustic terms we obtain the relations

$$\rho \frac{\delta \underline{v}}{\delta t} = -\rho V \frac{\delta \underline{v}}{\delta x} - \frac{\delta p}{\delta x} \tag{3}$$

and

$$\rho \frac{\delta \underline{v}}{\delta x} = -\frac{V}{c_o^2} \frac{\delta p}{\delta x} - \frac{1}{c_o^2} \frac{\delta p}{\delta t} \tag{4}$$

from which follows

$$\rho \frac{\delta \underline{v}}{\delta t} = \frac{M}{c_o} \frac{\delta p}{\delta t} - (1 - M^2) \frac{\delta p}{\delta x} \tag{5}$$

with the Mach number $M = V/c_o$.

From (4) and (5) follows the wave equation

$$\frac{\delta^2 p}{\delta t^2} = c_1 \cdot c_2 \frac{\delta^2 p}{\delta x^2} - 2V \frac{\delta^2 p}{\delta t \quad \delta x} \tag{6}$$

with

$$c_1 = c_o + V; \; c_2 = c_o - V.$$

A solution to (6) adjusted to our problem is

$$\underline{p}(x, t) = p_o [e^{-jk_1 x} + r\, e^{j(k_2 x + \phi)}] e^{j\omega t}. \tag{7}$$

From now on $\underline{p}$ is a complex quantity. In eq. (7) the first term is the plane wave propagating towards the orifice, the second term is the reflected wave with the reflection coefficient $r\, e^{j\,\phi}$. The wave numbers are:

$$k_1 = \omega/c_1 \text{ for the downstream propagation}$$
$$k_2 = \omega/c_2 \text{ for the upstream propagation.} \tag{8}$$

Without flow they would be replaced by

$$k_o = \omega/c_o\,. \tag{9}$$

Insertion of (7) into (5) leads to

$$\underline{v} = \frac{p_o}{Z} [e^{-jk_1 x} - r\, e^{j(k_2 x + \phi)}] e^{j\omega t} \tag{10}$$

with $Z = -\underline{\rho}\, c_o\,.$

From (7) and (10) the relation between the acoustic impedance of the orifice $\underline{W}$ and the reflection coefficient $r\, e^{j\,\phi}$ is

$$\underline{W} = \left( \frac{\underline{p}}{\underline{v}} \right)_{x=o} = Z \frac{1 + r\, e^{j\,\phi}}{1 - r\, e^{j\,\phi}}\,. \tag{11}$$

This equation is formally identical with that for the no-flow condition. (In (ref. 22) a different equation is obtained because the erroneous equation $\rho\ \delta v/\delta t = -\delta p/\delta t$ was used instead of eq. (5).

The evaluation of the reflection coefficient from the sound pressure node ratio $d = \underline{p}_{min}/\underline{p}_{max}$ and from the position of the sound pressure minima is anologous to that without flow. The small sound attenuation in the tube is taken into account by extrapolation of the measured values of $d(x)$ to $x=0$. Then the magnitude r of the reflection coefficient can be computed from

$$d_{x=o} = \frac{1 - r}{1 + r} \tag{12}$$

and the phase $\phi$ is obtained from

$$\phi = \pi \frac{-x_{min} - \Delta x/2}{\Delta x/2} \tag{13}$$

where $x_{min} \leqq 0$ is the position of the first pressure minimum nearest to the orifice and

$$\Delta x = (1 - M^2) \cdot \lambda_o/2 \text{ with } \lambda_o = c_o/f \tag{14}$$

is the absolute value of the distance of adjacent pressure minima.

### Influence of Curved Flow Profile

In contrast to the assumption made above that the flow velocity profile be flat, the real flow profile is curved. Using the equations (11), (12) and (13) the reflection coefficient and the radiation impedance can be computed without explicit appearance of the flow velocity. The only difficulty could arise, therefore, from a non-constant convection of the sound wave along the duct.

For the axial flow velocities $V_{ax} = 80$; 120 and 156 m/sec the distances of adjacent minima were measured along the entire measuring tube. The Mach number computed from eq. (14) proved to be constant within 1 per cent. For all axial flow velocities, $V_{ax}$, between 20 m/sec and 156 m/sec the distance of $\Delta x$ of adjacent pressure minima was given by eq. (14) if in the Mach number the velocity

$$V = 0.85\ V_{ax} \tag{15}$$

was used. By comparison with eq. (2) it can be concluded, that the sound field is convected with the average flow velocity, $\overline{V}$.

Therefore, the parameter used in the impedance measurements is the average flow velocity, $\overline{V}$, which is evaluated from the measured axial flow velocities, $V_{ax}$, by

$$\overline{V} = 0.85\ V_{ax}\,. \tag{16}$$

The average velocity is changed by the moving microphone probe by an amount smaller than 1 per cent.

## EXPERIMENTAL RESULTS FOR RADIATION IMPEDANCE

### Orifice in a Baffle

Three measuring tubes with the diameters $2a = 64$, 85, and 125 mm were mounted successively with the discharge orifice into the baffle. Magnitude and phase of the reflection coefficient were measured respectively. From them the resistance, R, and the reactance, X, of the radiation im-

pedance of the orifice were evaluated. The measurements cover the range of $k_o a$ between 0.15 and 1.8. The average flow velocities were $\overline{V}=0$, 34, 102, and 133 m/sec. With the tube of 125 mm diameter the highest available velocity was $\overline{V}=68$ m/sec. With the tube of 64 mm diameter, the measurements were impossible for velocities greater than 102 m/sec because of turbulent separation of the flow boundary layer at the inlet of the measuring tube.

The plots of the measured values for r, $\phi$, R and X indicate that these magnitudes are functions of $k_o a$ rather than functions of the frequency, f. They also depend on $\overline{V}$.

## The Reflection Coefficient of the Orifice

In Fig. 19 the magnitude of the reflection coefficient is plotted vs. $k_o a$ for the three tubes with the average flow velocity $\overline{V}$ as parameter. The corresponding points for the three tube diameters show rather good agreement with each other.

The influence of the flow becomes more evident if the magnitude of the reflection coefficient is normalized with the corresponding value without flow. In *Fig. 20* the ratio $r(k_o a, \overline{V}) / r(k_o a, 0)$ is plotted vs. $k_o a$. For sufficiently great values of $k_o a$ the normalized magnitude of the reflection

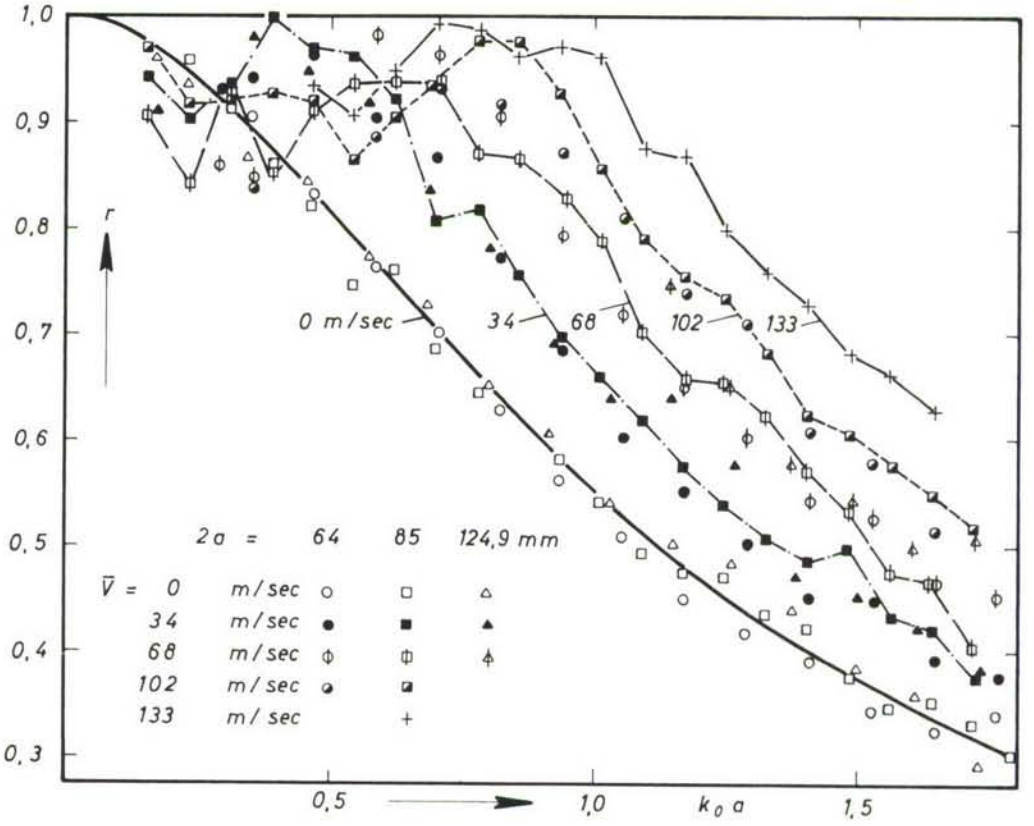


Fig. 19. Magnitude of reflection coefficient, r, for orifices of different diameters, 2a, in a baffle vs. $k_o a$. Parameter: flow velocity, $\overline{V}$.

coefficient becomes virtually independent from the frequency and depends linearly upon the average flow velocity, $\overline{V}$.

For low frequencies, however, the curves in Fig. 20 become rather complex. Furthermore, the measurements for these frequencies are not exactly reproducible. However, from the measurements it can surely be said that for these low values of $k_o a$ the magnitude of the reflection coefficient differs only slightly from unity.

With the magnitude of the reflection coefficient at zero flow velocity, $r(k_o a, 0)$, given the influence of the flow can easily be represented by the empirical relation

$$r(k_o a, \overline{V}) = \text{minimum}\,[1, r'(k_o a, \overline{V})] \tag{17}$$

where

$$r'(k_o a, \overline{V}) = r(k_o a, 0) \cdot \left( 1 + 2.0 \frac{\overline{V}}{c_o} \right)$$

The approximation curves according to this relation which yields straight lines are entered in Fig. 20.

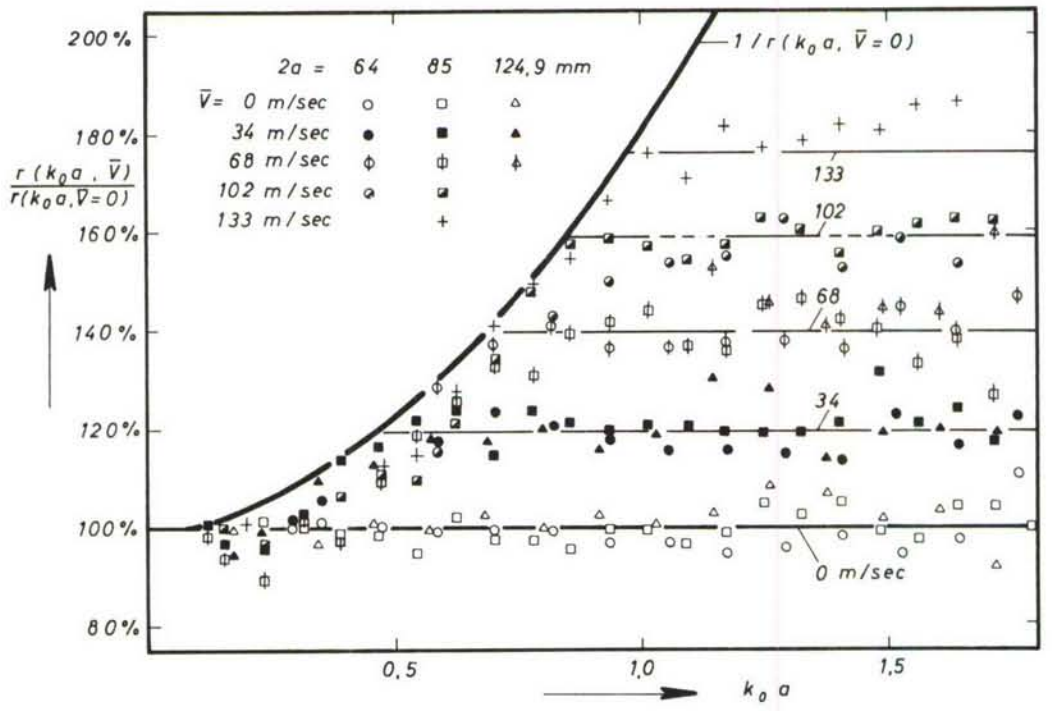


Fig. 20. Relative increase of the magnitude of the reflection coefficient of the orifices in a baffle compared with the value without flow.

The measured values for the normalized phase angle $\phi/\pi$ are plotted in *Fig. 21* together with the theoretical values for the no-flow case as functions of $k_o a$. Parameter is again the average flow velocity, $\overline{V}$. In general the phase angle is little affected by the superimposed air flow. For small values of $k_o a$ there is a small increase of the phase angle with increasing flow velocity. For greater values of $k_o a$ eventually present systematic variations of the phase angle with the flow velocity are within the error limits of the measurements. An uncertainty of 1.5 mm in the position of the pressure node corresponds to an error in $\phi$ of about 2.5 per cent at $k_o a = 0.8$ and of about 6 per cent at $k_o a = 1.6$.

For sake of clearness only the measurements for the tube with 85 mm diameter are entered in Fig. 21. The curves for the other diameters are identical within the error limits of these measurements.

## The Impedance of the Orifice

The resistance R of the available tube orifices divided by $\rho c_o$ is represented in *Fig. 22* as a function of $k_o a$ with the diameter and the average flow velocity, $\overline{V}$, as parameters. For higher values of $k_o a$ the superimposed air flow results in a parallel shift of the curves towards smaller values of $R/\rho c_o$. For small values of $k_o a$ the resistance of the orifice is lowered to values near zero.

The effect of the flow on the radiation resistance becomes clearer if

$$R(k_o a, \overline{V})/\rho c_o - R(k_o a, 0)/\rho c_o$$

is plotted as a function of $k_o a$ as it is done in *Fig. 23*. The resistance values without flow are from theory. On the right side of Fig. 23 the measured values for all tubes are near a constant

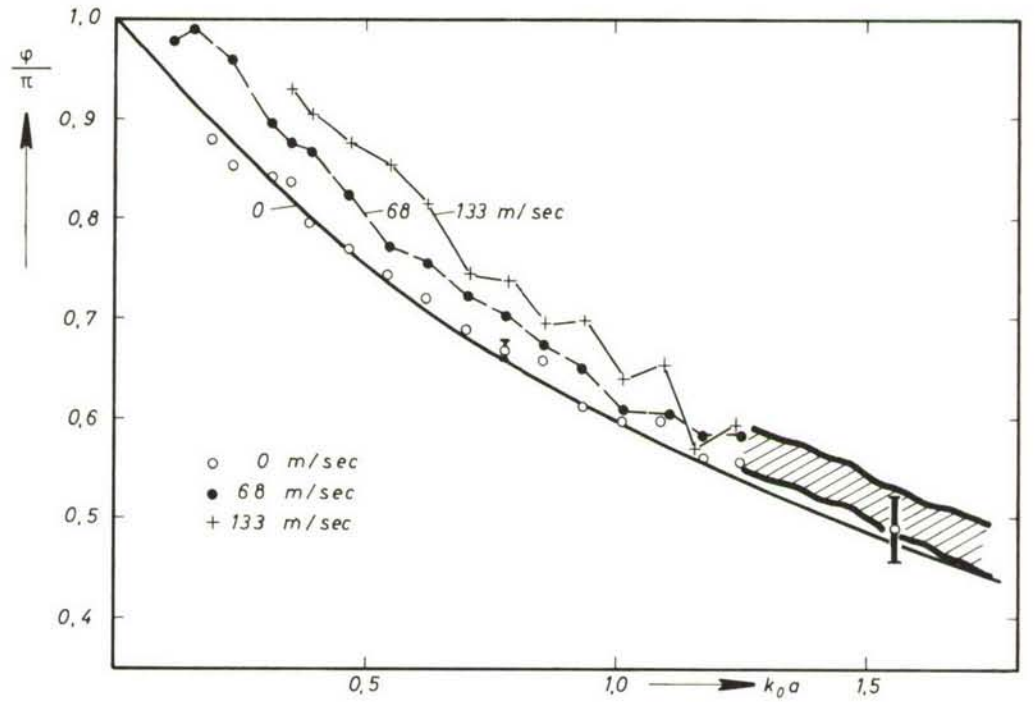


Fig. 21. Normalized phase, $\phi/\pi$, of the reflection coefficient of an orifice in a baffle vs. $k_o a$. Parameter: flow velocity, $\overline{V}$.

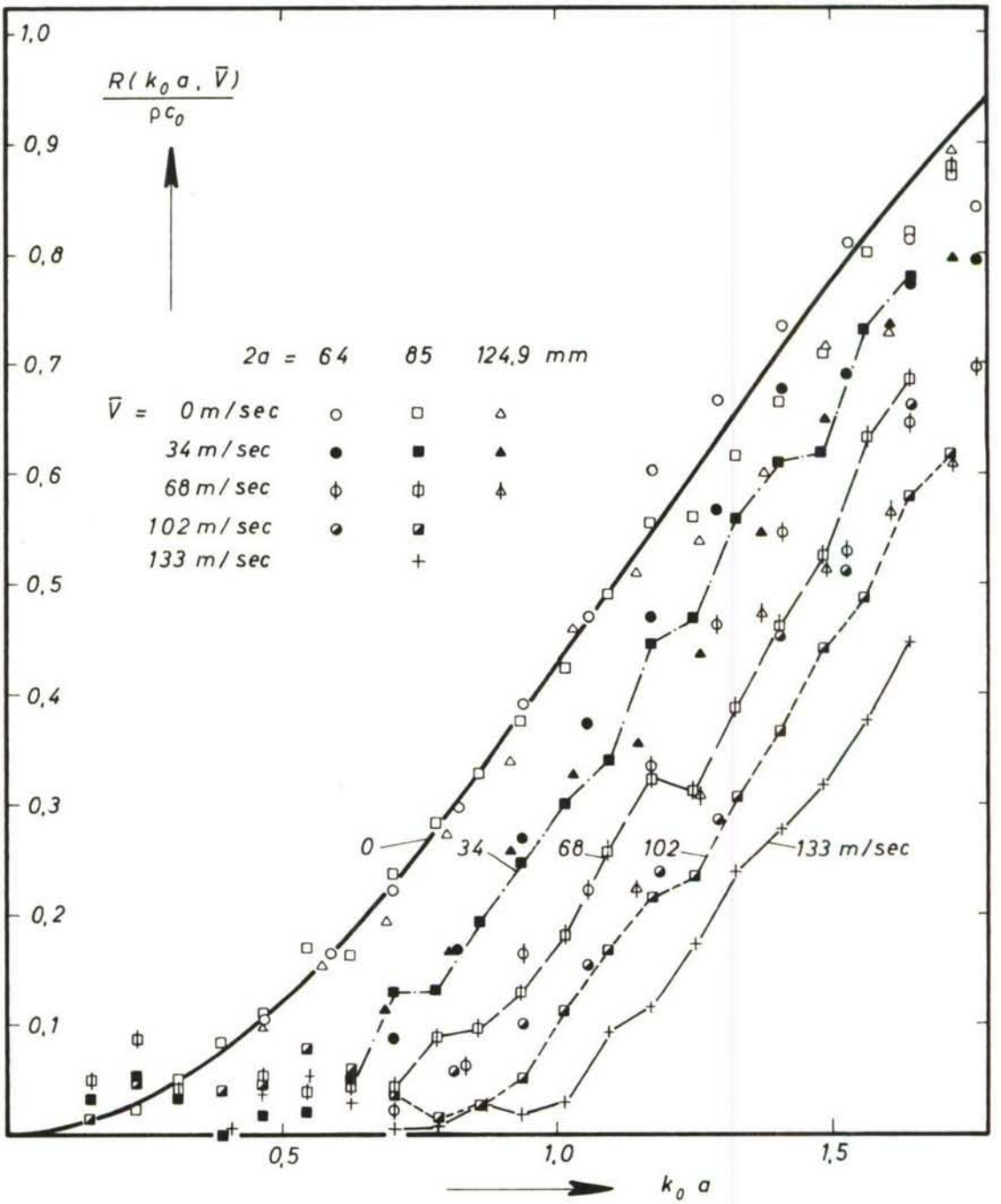


Fig. 22. Normalized resistance, $R/\rho c_o$, of orifices with different diameters 2a in a baffle vs. $k_o a$. Parameter: flow velocity, $\overline{V}$.

ordinate value for a constant flow velocity. The measurements are reproducible within a horizontal strip of $\pm 0.05\ \rho c_o$. Therefore, the empirical relation holds:

$$R(k_o a, \overline{V})/\rho c_o = \text{Maximum}\,[O, R'(k_o a, \overline{V})/\rho c_o] \tag{18}$$

with

$$R'(k_o a, \overline{V})/\rho c_o = R(k_o a, 0)/\rho c_o - 1 \cdot 1 \frac{\overline{V}}{c_o} \cdot$$

This relation represents also the measurements for small values of $k_o a$.

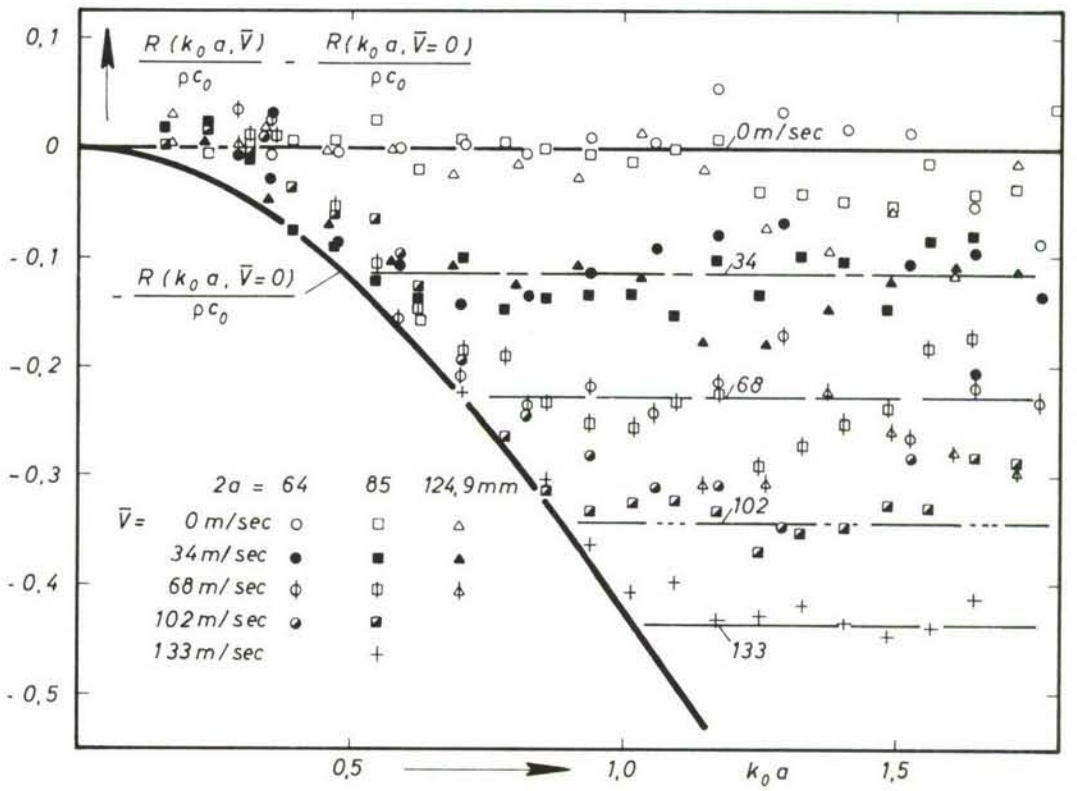


Fig. 23. Change of the resistance of an orifice with flow discharge compared with an orifice without flow for different diameters, 2a together with approximate curves according to eq. (18). Parameter: flow velocity.

The ratio of the reactance, X, with $\rho c_o$ for the tube with 85 mm inner diameter is plotted in *Fig. 24* as a function of $k_o a$. The measurements with the other tubes coincide with the values of Fig. 24, i.e., the reactance, too, depends on $k_o a$ rather than on the frequency, f. The variation of the reactance is caused at low values of $k_o a$ mainly by the change of the phase angle, $\phi$, of the reflection coefficient and at high values of $k_o a$ mainly by the change of the magnitude of the reflection coefficient.

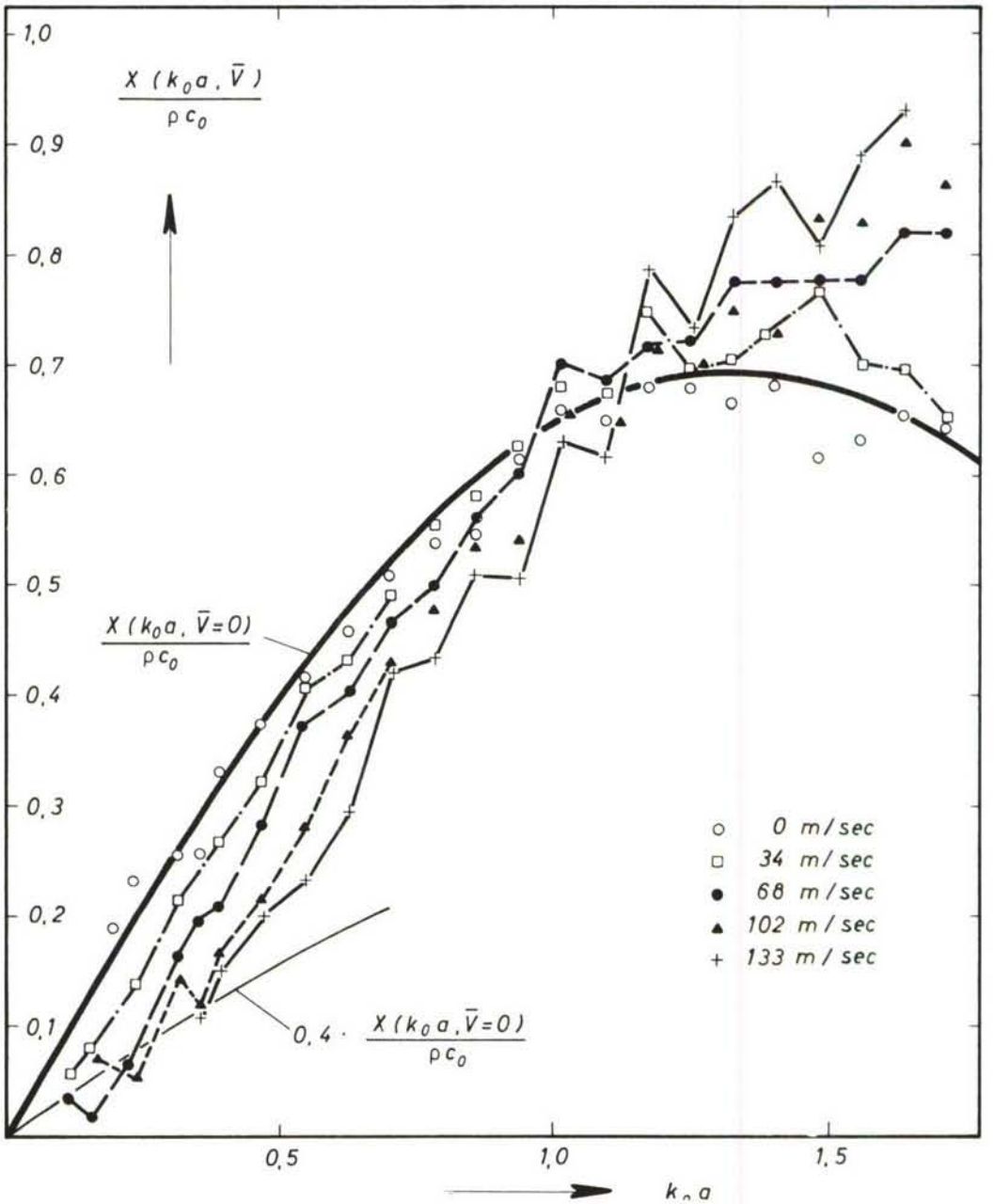


Fig. 24. Normalized reactance, $X/\rho c_o$, of an orifice with diameter $2a = 85$ mm in a baffle vs. $k_o a$. Parameter: flow velocity, $\overline{V}$.

### Free Orifice

The impedance measurements were repeated for the tube with 85 mm diameter without the baffle, the discharge orifice radiating freely into the measuring room. The reflection coefficient and the radiation impedance of the orifice were changed by the flow discharge qualitatively in the same manner as with the baffle. The relation obtained from the measurements with the baffle for the radiation resistance holds here, too, if the values of $R(k_o a, 0)/\rho c_o$ for the orifice without baffle are used.

### Variation of Wave Number

Without flow the reflection coefficient and the radiation impedance of an orifice are functions of $k_o a$ only. It is, therefore, an obvious suggestion to try to take the flow discharge into account by a proper transformation of the axis of the wave numbers. The maximum correction is obtained in the range of the wave numbers investigated in this paper when $k_o a = \omega/c_o$ is replaced by $k_1 = \omega/(c_o + \overline{V})$. Therefore, the results of measurement were plotted vs. $k_1 a$ instead of $k_o a$ used up to now. This corresponds to a transformation of the abscissa according to

$$k_1 a = \frac{1}{1 + V/c_o} \cdot k_o a \,. \tag{19}$$

The independence of the measured quantities from the tube diameter is preserved by this transformation.

As an example, the resistance of the discharge orifice in the baffle is plotted vs. $k_1 a$ in *Fig.* 25. Only for high values of $k_1 a$ does the measured curves coincide with the theoretical curve without flow. For low values of $k_1 a$ there remain distinct systematical differences. The same statement holds for the reflection coefficient. Even at high $k_1 a$ values the coincidence of the curves is obtained only for the reflection coefficient and the resistance. The phase angle (see Fig. 21) and the reactance, X, (see Fig. 24), however, cannot be matched by the introduction of the abscissa, $k_1 a$.

## VARIATION OF PARAMETERS

The influence of some flow parameters on the reflection coefficient and the radiation impedance was investigated for the 85 mm diameter orifice.

### Increase of Turbulence Level

The intention of the following experiments was to increase the turbulence level in the orifice or behind it without introduction of rigid barriers into the flow. Thereby flow contractions with associated static pressure drops and eventual acoustic control of the boundary layer separation at the obstacles were to be avoided.

First, the turbulence level in the orifice was increased by a compressed-air jet blown into the measuring tube 80 cm ahead of the orifice. By these means the turbulence level in the center of the orifice was raised from 1.5 to 5.5 per cent (at the average flow velocity, $\overline{V}$=51 m/sec). The reflection coefficient measured under these conditions in the $k_o a$ range between 0.8 and 1.6 was in the mean about 1 per cent smaller than with the low turbulence level. These deviations are, however, within the error limits of the measurements.

In a second experiment the compressed-air jet was blown into the air jet behind the discharge orifice. By these means the turbulence level 25 mm behind the orifice was raised from about 4 per cent to about 20 per cent in one-third of the jet area. Here again the measurements

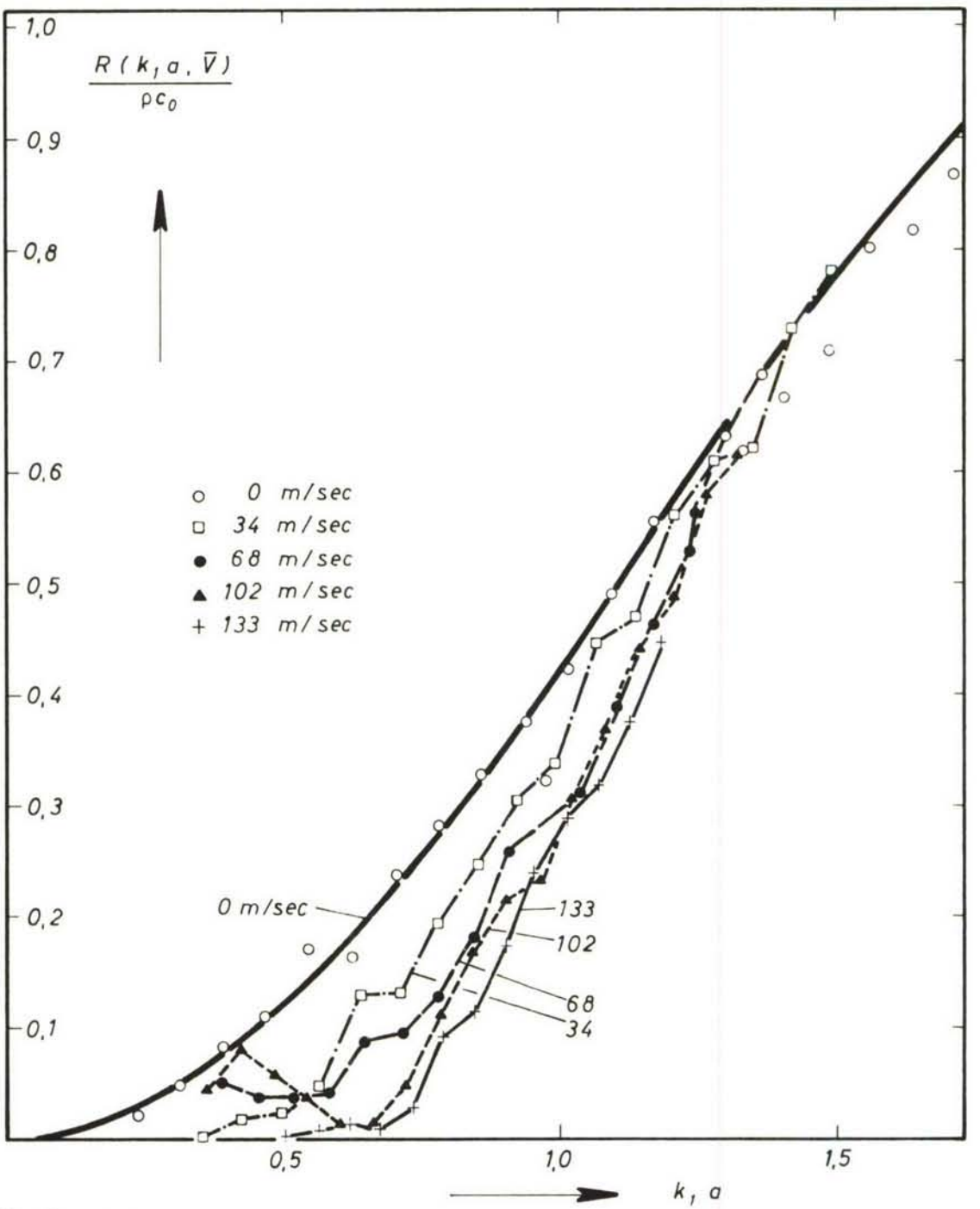


Fig. 25. Resistance, R, of the orifice with diameter 2a = 85 mm in a baffle as a function of $k_1a$. Parameter: flow velocity, $\overline{V}$.

of the magnitude of the reflection coefficient showed only small systematical variations of about 2 per cent.

From these measurements it may be concluded that the experimental results reported in Section IV. are valid for higher turbulence levels, too.

## Guided Flow Discharge

The intention of the next experiment was to investigate the importance of the shape of the air jet behind the discharge orifice with respect to the acoustical radiation. The object was therefore to change the shape of the air jet without changing markedly the acoustic qualities of the orifice without flow.

This was achieved by a perforated guide tube 150 cm in length with the inner diameter of the measuring tube mounted behind the discharge orifice. The air flow remained virtually within the guide tube along its entire extension. The width of the air jet 1 cm behind the guide tube was about 6 per cent greater than the inner tube diameter compared to about 500 per cent without the guide tube. Since for most frequencies the end of the guide tube is several wavelengths away from the discharge orifice of the measuring tube, the air jet by these means keeps a constant cross section within the acoustic near field of the radiating orifice.

Without flow the magnitude of the reflection coefficient of the orifice of the measuring tube is not changed by the guide tube. The magnitude of the reflection coefficient was measured for average flow velocities, $\overline{V}$, between 0 and 127 m/sec with the $k_0a$ range between 0.35 and 1.7. The superposition of the flow changes the magnitude of the reflection coefficient in the same direction as without guide tube, i.e., the reflection coefficient is increased with the flow velocity. This increase, however, is only about half as much as without guide tube.

These results indicate that the shape of the jet behind the discharge orifice has some influence upon the sound radiation from the orifice.

## Nozzle for Increased Flow Mixing of the Jet

A nozzle having a truncated cone with a rectangular corner protruding into the flow end of virtually constant cross sectional area (see Fig. 27) was mounted on the measuring tube. Having

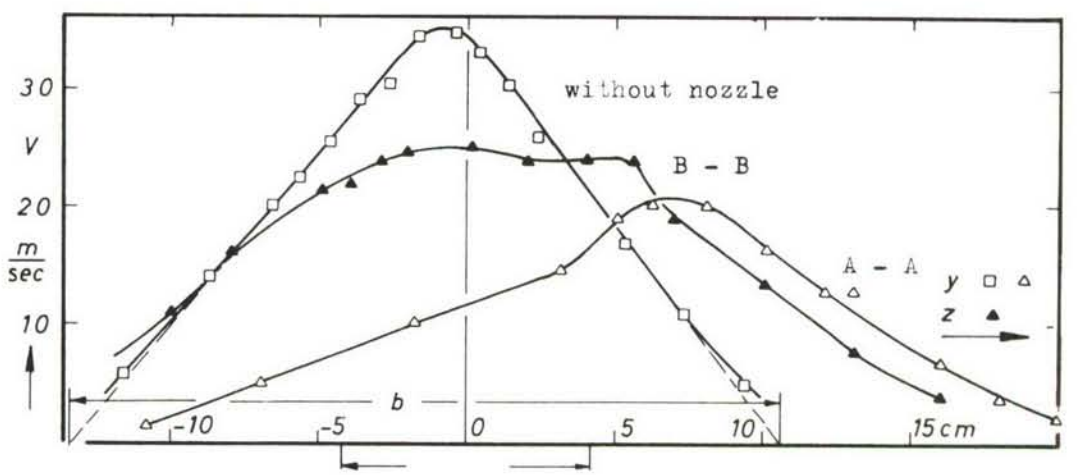


Fig. 26. Flow velocity profiles in the air jet behind the nozzle. Average flow velocity in the measuring tube $\overline{V}$=51 m/sec.

this design, the static pressure drop along the nozzle remains small, e.g., it is p=3 mm Hg at $\overline{V}$=102 m/sec compared with p=2 mm Hg along a section of equal length of the smooth measuring tube.

The effect of the nozzle was a much greater mixing of the jet behind the nozzle. The profiles of the flow velocity in *Fig. 26* show an increase of the jet diameter b of about 35 per cent. Furthermore, very high turbulence levels (greater than 40 per cent) are obtained in areas with a high mean flow velocity, this, too, indicating an increased mixing.

In the measurements of the magnitude of the reflection coefficient the plane of reference was the entrance plane E of the nozzle. The points in *Fig. 27* show the results of measurement. They are compared with the curves taken from the measurements with the free unflanged orifice. Although the mixing behind the nozzle is much greater than behind the free orifice there are no systematical deviations between the two measurements.

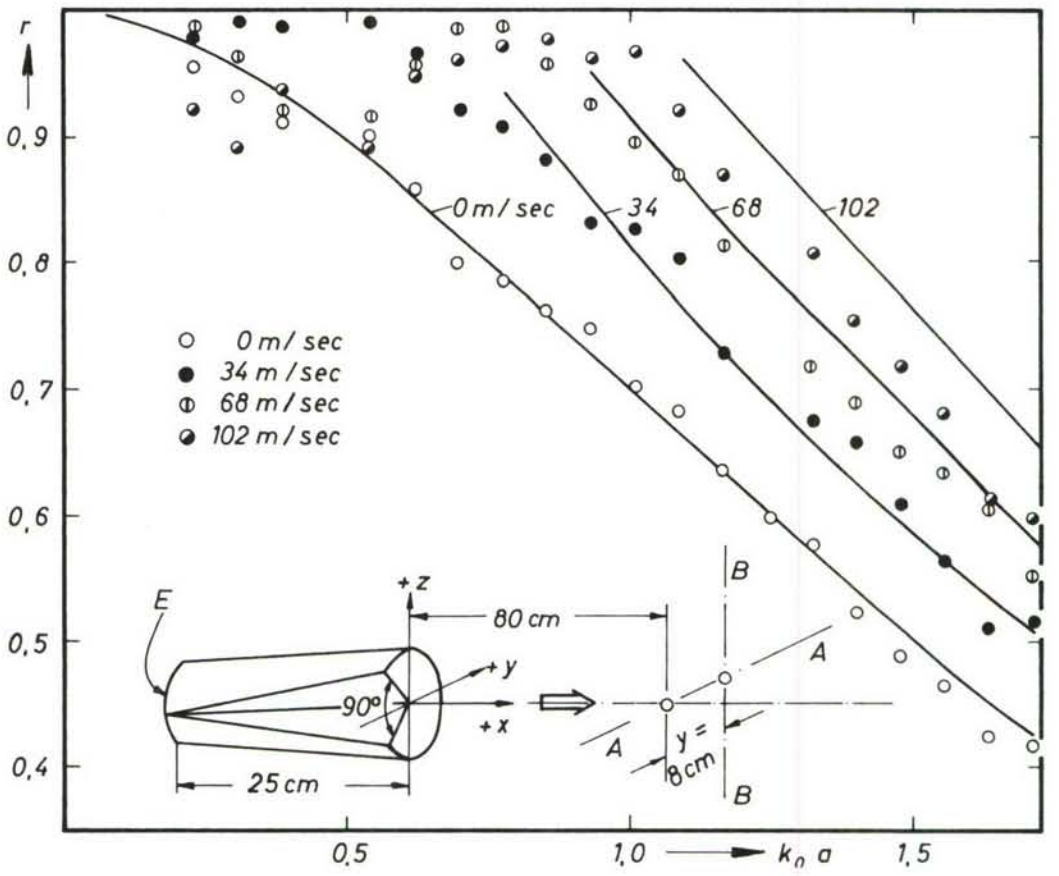


Fig. 27. Measured values of the magnitude of the reflection coefficient, r, of the nozzle. Parameter: flow velocity, $\overline{V}$, in the measuring tube. For comparison: curve of the same quantity without nozzle.

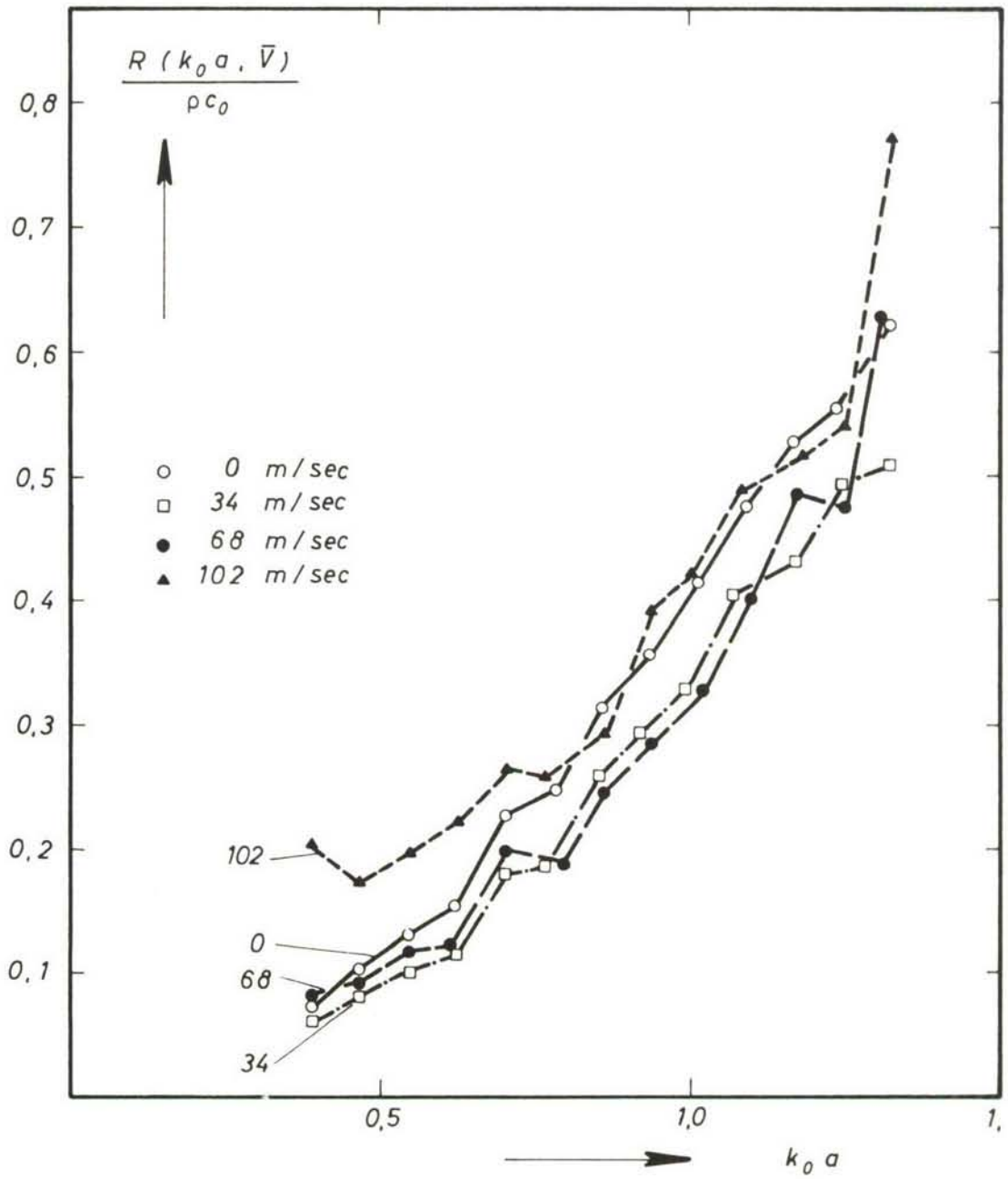


Fig. 28. Normalized resistance, $R/\rho c_o$, of an orifice in a baffle with fence No. 5 inserted vs. $k_o a$. Parameter: flow velocity, $\bar{V}$.

## Fence and Diaphragm in Orifice

Fences made of cylindrical wires in a symmetrical arrangement were mounted into the plane of the orifice of the tube with 85 mm inner diameter. The arrangement of the fences is shown in Fig. 29. In all measurements the orifice was mounted into the baffle. In Table II the wire diameters and the surface coverage (ratio of wire surface to orifice surface) are tabulated.

TABLE II.

*Wire Diameter and Surface Coverage of Fence*

| Fence No. | No. 1 | No. 2 | No. 4 | No. 5 | No. 6 |
|---|---|---|---|---|---|
| Surface Coverage | 0.07 | 0.11 | 0.20 | 0.29 | 0.29 |
| Wire Diameter | | 2 mm | | 3 mm | 4 mm |

The turbulence level behind the fences increases with the surface coverage. The width of the jet is not much changed by the fences. The fences result in a flow contraction in the plane of the orifice and immediately behind it. This is associated with a drop of the static pressure across the reference plane of the measurements. Thus an acoustically effective resistance appears which is the differential quotient of the static pressure drop, $\Delta p$, in the plane of the orifice with the average flow velocity, $\overline{V}$,

$$R_{flow} = \frac{d(\Delta p)}{d\overline{V}} \quad . \tag{20}$$

In these experiments the term "acoustic impedance" will always stand for the ratio $\underline{W} = \underline{p}/\underline{v}$ where $\underline{p}$ is the sound pressure and $\underline{v}$ is the acoustic particle velocity in the reference plane. In Fig. 28 the resistance of the orifice is represented as a function of $k_o a$ for fence No. 5. The curves for different flow velocities are approximately coincident. A comparison with Fig. 22 for the orifice without fence shows a strong reduction of the influence of the flow. The effect of increasing surface coverage can be seen from *Fig 29* where the magnitude of the reflection coefficient with the different fences is plotted vs. flow velocity. The measurements were performed for a medium constant value of $k_o a = 0.937$. Fences No. 5 and No. 6 are of the same surface coverage. Fence No. 6 has, however, the greater static pressure drop.

The measurements with fence No. 6 yielded remarkable results for the resistance at low frequencies. They are plotted in *Fig. 30*. There the resistance with flow is distinctly greater than without flow. The resistance at low values of $k_o a$ increases with increasing flow velocity. The decrease of the resistance at the free orifice is even overcompensated by the fence. It should be stated, however, that the resistance without flow is nearly unchanged by the fence.

The turbulence induced by the insertion of the fence cannot be considered to be the origin of this behaviour. As it is shown in *Fig. 31* the turbulence level with fence No. 5 is comparable to that with the compressed-air jet in former experiments. In those measurements, with the flow disturbance by a compressed-air jet, the increased turbulence level was virtually ineffective. Also a frequency analysis of the turbulence with the grid showed no peculiarities at the low frequencies where the refection coefficient is changed greatly.

The following measurements indicate that the reason of the increase of the magnitude of the reflection coefficient with the fences of high surface coverage can be found in the flow contraction, i.e., in the static pressure drop at the reference plane of the measurements.

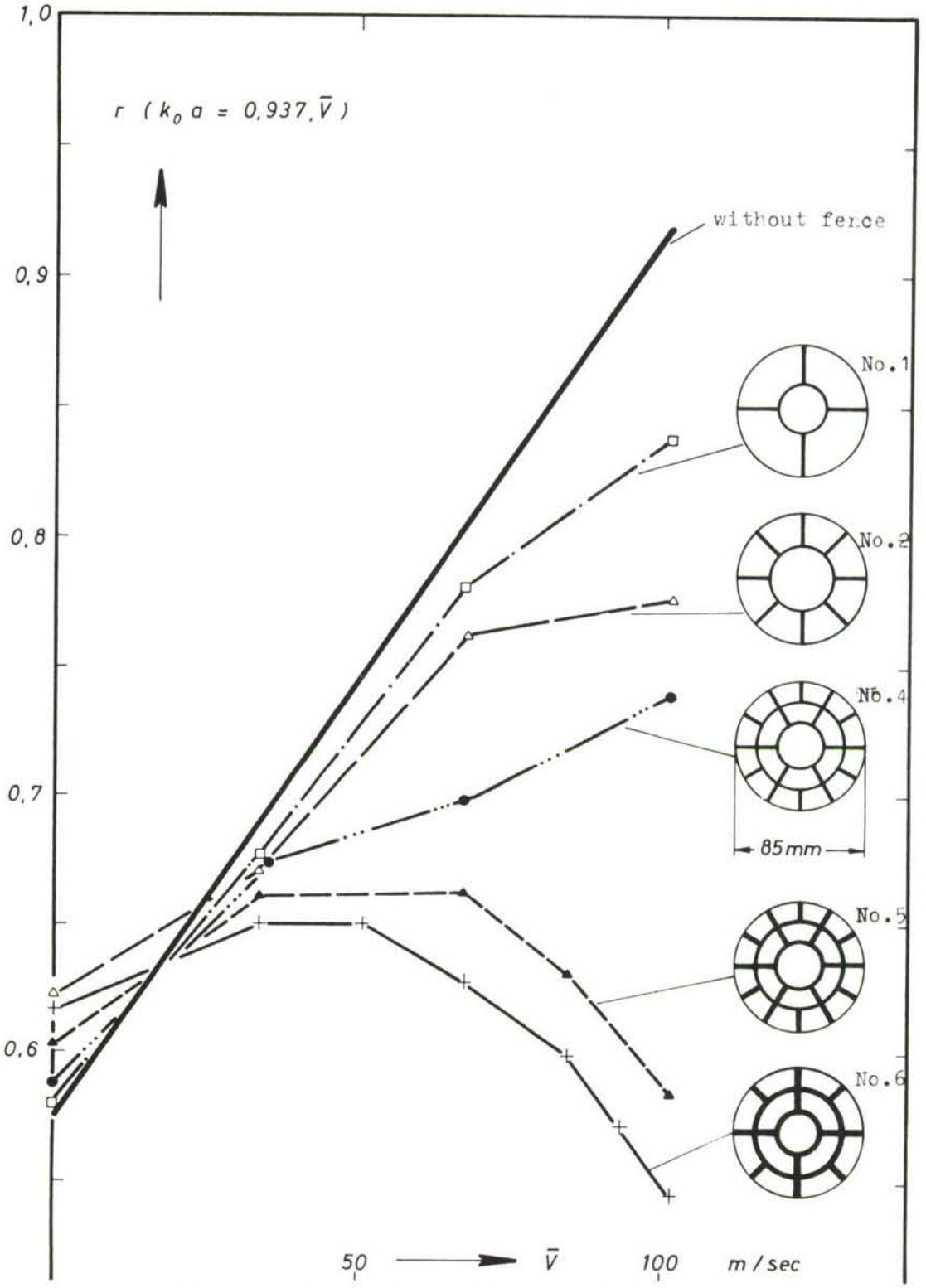


Fig. 29. Magnitude of the reflection coefficient, r, of an orifice in a baffle with several fences inserted vs. flow velocity, $\bar{V}$, at $k_o a = 0.937$.

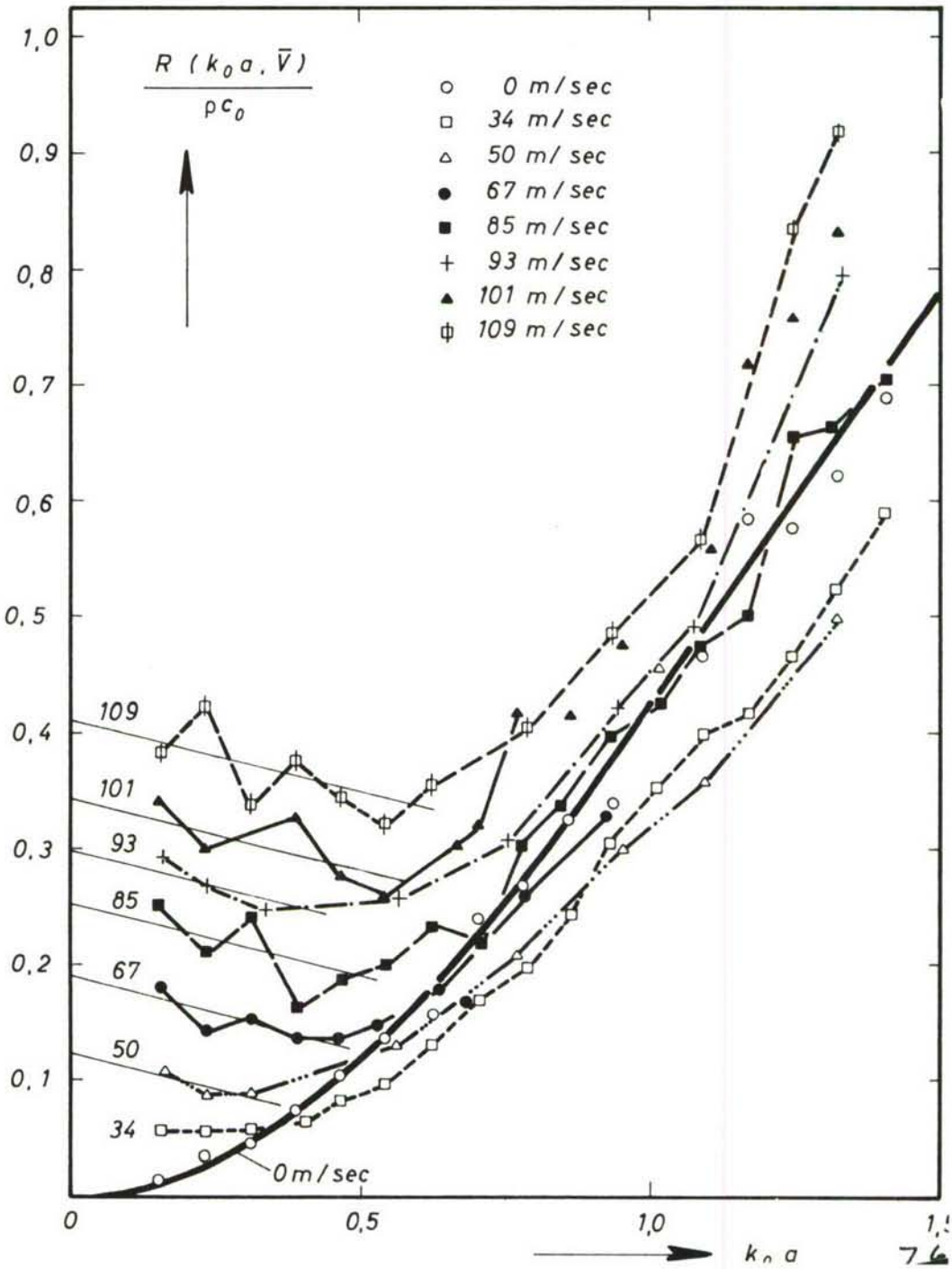


Fig. 30. Normalized resistance, $R/\rho c_0$, of an orifice in a baffle with fence No. 6 inserted. For comparison: resistance without fence and without flow.

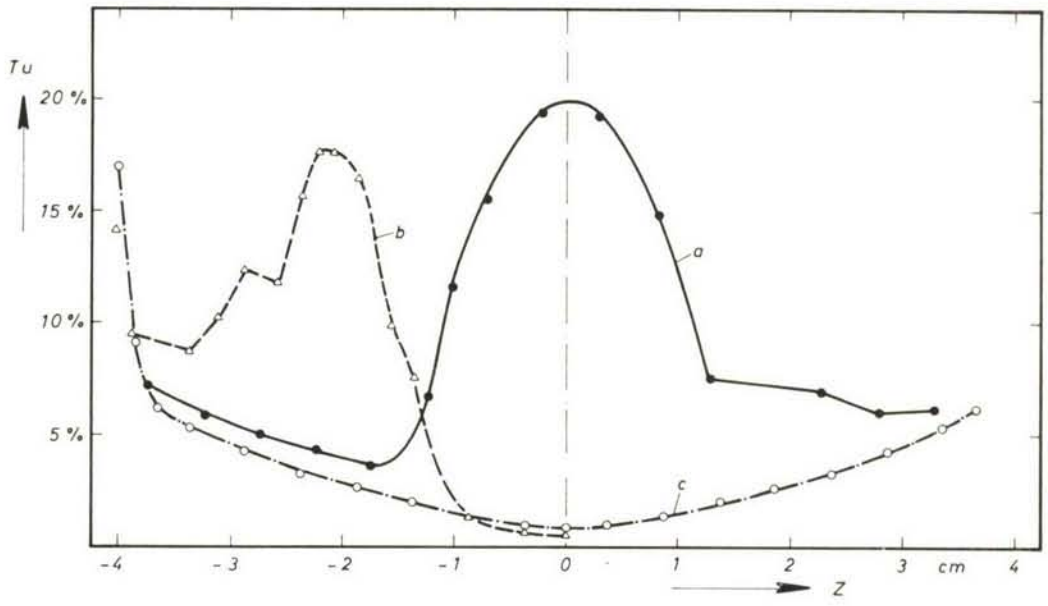


Fig. 31. Turbulence level, Tu, in the jet 25 mm behind the orifice plotted vs. position, z, (see Fig. 27)
a) with compressed-air blown into the jet near the orifice
b) with fence No. 5 inserted
c) with undisturbed orifice

In these measurements circular diaphragms were inserted into the orifice. The diaphragms had apertures of different diameters. *Table III* gives the surface coverage, the discharge coefficient, $\mu$, according to (ref. 23) and the measured discharge coefficient of the different diaphragms.

TABLE III.

*Diaphragm Characteristics*

| Diaphragm No. | No. 7 | No. 8 | No. 9 |
|---|---|---|---|
| Surface Coverage q | 0.29 | 0.39 | 0.49 |
| $\mu$ from ref. 23 | — | 0.75 | 0.71 |
| $\mu$ measured | 0.63 | 0.70 | 0.68 |

*Fig. 32* shows the resistance of the orifice with a diaphragm inserted. Parameter is the average flow velocity in the measuring tube. Once again the resistance increases at low frequencies when the flow velocity is raised. This can be explained by the addition of the differential flow resistance to the acoustic resistance according to eq. (20).

An argument for this explanation would be if the differential flow resistance could be obtained, too, from the acoustic measurements by extrapolation to zero frequency.

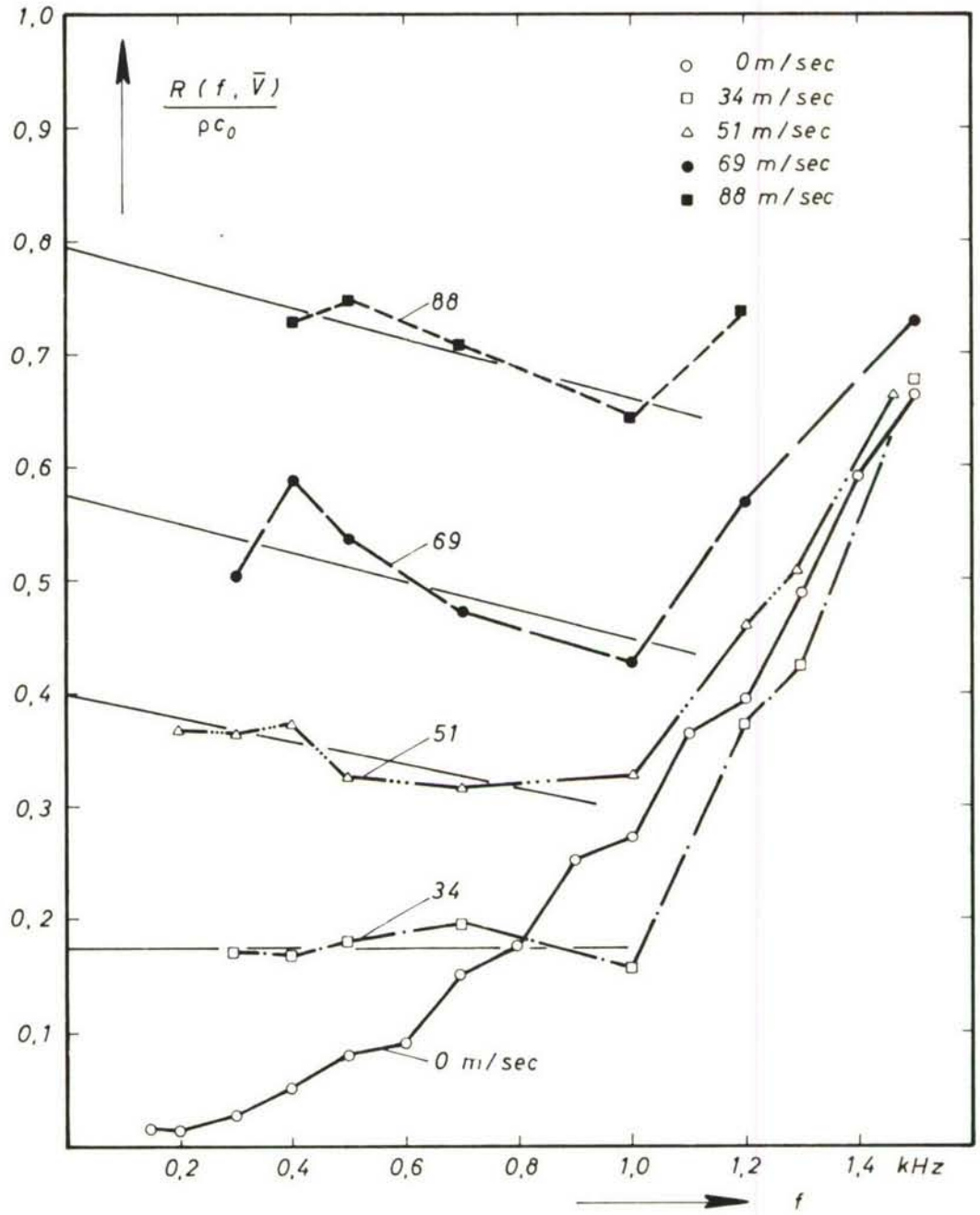


Fig. 32. Resistance, R, of an orifice with a diaphragm (No. 7) inserted vs. signal frequency, f. Parameter: flow velocity, $\overline{V}$.

The differential flow resistance, $R_{flow}$, can be determined directly according to eq. (20) or from the equation

$$\frac{R_{flow}}{\rho c_0} = \frac{\overline{V}}{c_0}\left[\left(\frac{1}{1-q}\,\frac{1}{\mu}\right)^2 - 1\right] \qquad (21)$$

The experimental results are given in *Fig. 33*, where the pressure drop, $\Delta p$, is plotted and in *Fig. 34* where the flow resistance obtained by graphical differentiation is represented by the curves in that figure.

On the other hand the extrapolation values from the acoustic measurements of the resistance to zero frequency are entered as points. They agree within the error limits of the measurement with the curves. The accuracy of the extrapolation can be estimated from Fig. 30 and Fig. 32.

These results are an approval of the hypothesis pronounced above that the increase of the acoustically measured flow resistance of an orifice with rigid obstacles of sufficiently great surface coverage at low frequencies comes from the addition of the differential flow resistance.

## CONCLUSIONS

The reported results show that the impedence of a tube orifice is changed by flow discharge through the orifice. With undisturbed orifices, or more precisely, with orifices without rigid obstacles leading to flow contraction, the radiation resistance is decreased by the superimposed flow. Empirical formulas could be given for this decrease. Also the reflection coefficient is unaffected

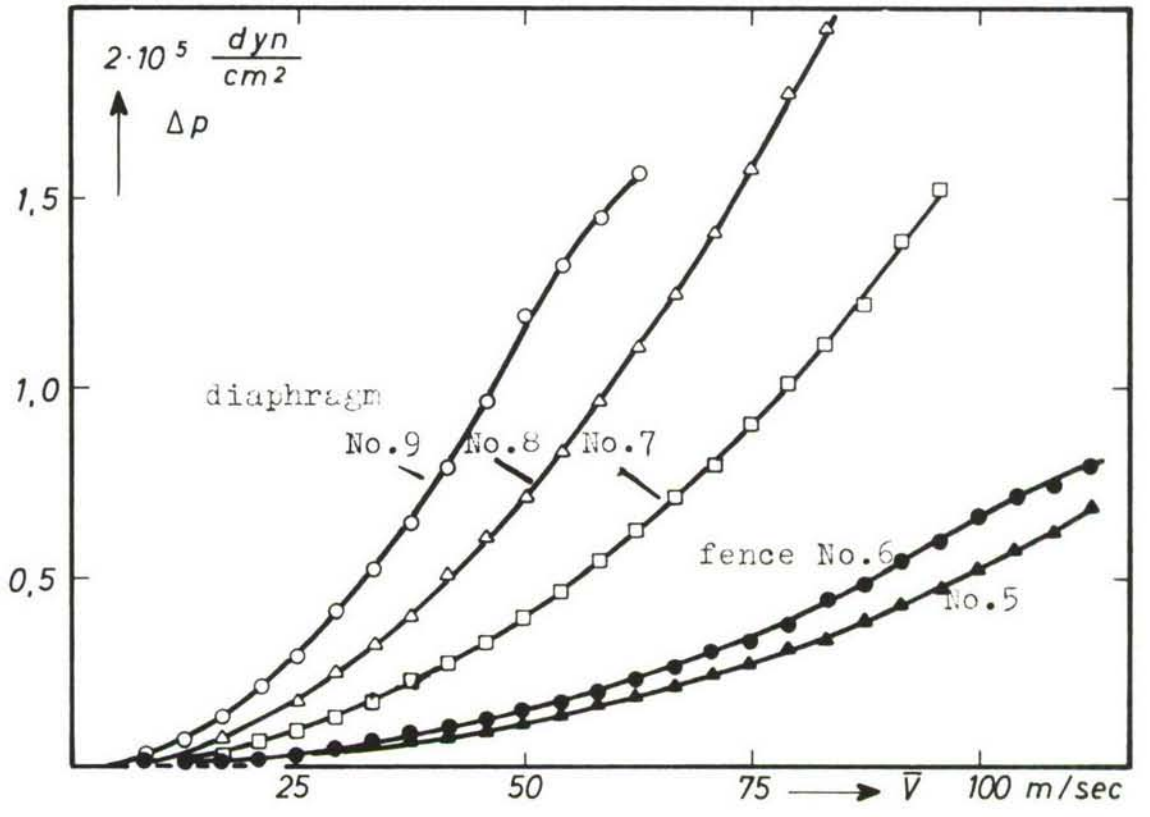


Fig. 33. Static pressure drop, p, vs. flow velocity, $\overline{V}$.

by changes of the turbulence level of the flow, and the sound radiation is affected by the shape of the jet behind the orifice.

With rigid obstacles in the orifice leading to static pressure drops in the plane of the orifice the acoustically measured resistance is increased by the flow at low frequencies. This increase could be explained by the additive term of the differential flow resistance.

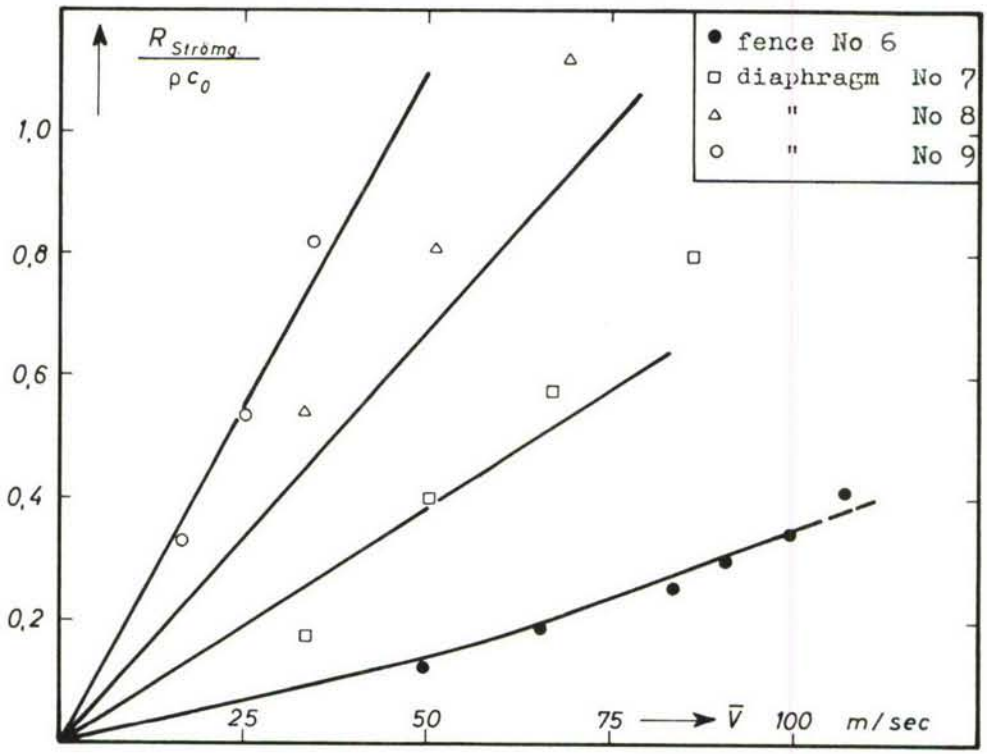


Fig. 34. Differential flow resistance, R. from acoustic measurements (points) and from static measurements (curves) vs. flow velocity, $\overline{V}$.

The measurements up to now give no explanation for the change of the impedance of orifices without static pressure drop. Additional research should be conducted to determine the influence of the flow discharge on the directivity pattern of the sound radiation. Another question would be how the acoustic impedance of a flow inlet would be affected by the flow.

# References


1. Barthel, F., "Untersuchungen uber nichtlineare Helmholtzresonatoren," (Investigations on Nonlinear Helmholtz Resonators) *Frequenz*, vol. 12, p. 72, 1958.

2. Becker, E., *DVL-Bericht*, vol. 132, 1960.

3. Benjamin, T. B., *J. Fluid. Mech.*, vol. 6, p. 161, 1959.

4. Brekhovakich, L. M., *Soviet Phys. Acoust.*, vol. 2, p. 247, 1956.

5. Heller, G. S., *J. Acoust. Soc. Am.*, vol. 25, p. 950, 1953.

6. Hutte, *"Des Ingenieurs Taschenbuch"* (The Engineers Handbook), "I Theroretische Grundlagen" (Theoretical Groundwork), S. 799 ff, Flüssigkeitsstrahlen (Fluid Jets), Berlin, 1955.

7. Ingard, U., Attenuation and Regeneration of Sound in Ducts and Jet Diffusers, Chapter: Energy Transmission Coefficient, *J. Acoust. Soc. Am.*, vol. 31, p. 1202, 1959.

8. Ingard, U., "On the Theory and Design of Acoustic Resonators," *J. Acoust. Soc. Am.*, vol. 25, p. 1037, 1953.

9. Kornhauser, E. T., *J. Acoust. Soc. Am.*, vol. 25, p. 945, 1953.

10. Kosten, C. W., "Rohrmessungen bei Senkrechtem Einfall" (Measurements on Pipes at Perpendicular Incidence), *Proceedings of the Third International Congress on Acoustics* (German) Stuttgart, vol. 2, p. 817, 1959.

11. Lutz, O., Resonanzschwingungen in den Rohrleitungen von Kolbenmaschinen (Resonance Vibrations in the Ducts of Piston Engines) Berichte aus Labor. f. Verbrennungskraftmaschinen d. T. H. Stuttgart, H. 3, p. 17, 1934.

12. Martin, H., Die Dämpfung der akustischen Ein- und Ausschwingungsvorgänge und der Resonanzüberhöhung durch den Abgasgleichstrom in Abgasanlagen (The Damping of the Acoustic Transients and the Resonance Amplification by the Exhaust D C Stream in Exhaust Systems) Motortechn. Zeitschr, vol. 22, 1961.

13. Mechel, F., P. Mertens, and W. Schilz, *Research on Sound Propagation in Sound-Absorbent Ducts with Superimposed Air Streams*, AMRL-TDR-62-140, volumes III and IV, 6570th Aerospace Medical Research Laboratories, Wright-Patterson Air Force Base, Ohio, December 1962, AD296946, AD296985, AD296984, and AD431012.

14. Mechel, F. and P. Mertens, "Schallausbreitung in Absorbierend Ausgekleideten Strömungskanälen Bei Hohen Windgeschwindigkeiten" (Propagation of Sound in Absorbing Ducts at High Stream Velocities) *Acustica* (German), vol. 13, No. 3, p. 154, 1963.

15. Mechel, F., "Schalldämpfung und Schallverstärkung in Luftströmungen Durch Absorbierend Ausgekleidete Kanäle" (Sound Attenuation and Amplification in Air Streams Through Ducts With Absorbent Walls) *Acustica* (German), vol. 10, p. 133, 1960.

16. Meyer, E., F. Mechel, G. Kurtze, "Experiments on the Influence of Flow on Sound Attenuation in Absorbing Ducts," *J. Acoust. Soc. Am.*, vol. 30, p. 165, 1958.

17. Powell, A., "Theory of Sound Propagation Through Ducts Carrying High-Speed Flows," *J. Acoust. Soc. Am.*, vol. 32, p. 1640, 1960.

18. Schliz, W., *Acustica*, vol. 11, p. 137, 1961.

19. Schlichting, H., *Grenzschichttheorie* (Boundary Layer Theory), Chap. XVI, Karlsruhe, 1958.

20. Schlichting, H., *Grenzschichttheorie* (Theory of Boundary Layer Flow), Chap. XX, Karlsruhe, 1958.

21. Scott, R. A., "An Apparatus for Accurate Measurement of the Acoustic Impedance of Sound Arbsorbing Materials," *Proc. Phys. Soc.*, vol. 58, p. 253, 1946.

22. Trimmer, J. D., "Sound Waves in a Moving Medium," *J. Acoust. Soc. Am.*, vol. 9, p. 162, 1937.

23. Weisbach, J., Lehrbuch der Ingenieur- und Maschinen-Mechanik, 5. Auflage. 1. Teil: Theoretische Mechanik. 443 Ausfluss des Bewegten Wassers (Part I: Theoretical Mechanic, paragraph 443, Out-Flow of Moving Water), Braunschweig, 1896.

24. Westervelt, P. J., P. W. Sieck, "The Correlation of Non-Linear Resistance, Flow Resistance, and Differential Resistance for Sharp-Edged Circular Orifices (Abstract), *J. Acoust. Soc. Am.*, vol. 22, p. 680, 1950.

25. Westervelt, P. J., "Acoustic Impedance in Terms of Energy Functions and the Nonlinear Reactance of Orifices (Abstract), *J. Acoust. Soc. Am.*, vol. 23, p. 630, 1951.

26. Westervelt, P. J., "Acoustical Impedance in Terms of Energy Functions," *J. Acoust. Soc. Am.*, vol. 23, p. 347, 1951.

Security Classification

**DOCUMENT CONTROL DATA - R&D**

*(Security classification of title, body of abstract and indexing annotation must be entered when the overall report is classified)*

1. ORIGINATING ACTIVITY *(Corporate author)*
III. Physiklaisches Institut der Universitat Gottingen
Gottingen, Germany

2a. REPORT SECURITY CLASSIFICATION
UNCLASSIFIED

2b. GROUP
N/A

3. REPORT TITLE
INTERACTION BETWEEN AIR FLOW AND AIRBORNE SOUND IN A DUCT

4. DESCRIPTIVE NOTES *(Type of report and inclusive dates)*
Final report, February 1963 - January 1964

5. AUTHOR(S) *(Last name, first name, initial)*
Mechel, F. P.
Mertens, P. A.
Schilz, W. M.

| 6. REPORT DATE | 7a. TOTAL NO. OF PAGES | 7b. NO. OF REFS |
|---|---|---|
| September 1965 | 58 | 26 |

| 8a. CONTRACT OR GRANT NO. | 9a. ORIGINATOR'S REPORT NUMBER(S) |
|---|---|
| AF 61(052)-666 | |
| b. PROJECT NO. 7231 | |
| c. Task No. 723104 | 9b. OTHER REPORT NO(S) *(Any other numbers that may be assigned this report)* |
| d. | AMRL-TR-65-53 |

10. AVAILABILITY/LIMITATION NOTICES
Distribution of this document is unlimited.

| 11. SUPPLEMENTARY NOTES | 12. SPONSORING MILITARY ACTIVITY |
|---|---|
| | Aerospace Medical Research Laboratories, Aerospace Medical Div., Air Force Systems Command, Wright-Patterson AFB, Ohio |

13. ABSTRACT

Several studies of the interaction between air flow and airborne sound in a duct have been made. Three projects were investigated: (1) The excitation of boundary layer distortions in a laminar boundary layer by simulated oscillatory flexural waves was investigated. Results show boundary layer waves are excited whenever the phase velocity of the flexure wave is in the instability range of the phase velocity of boundary layer waves. (2) The propagation of a pressure pulse wave front and the acoustic impedance of porous absorbers are examines in ducts with air flow. Measurements prove the sound energy of the wave front is directed towards the walls and the absorber impedance becomes nonlinear when the absorber is penetrated by the flow. (3) The effect on the acoustic radiation impedance of an orifice with flow discharge restricted by fences and diaphragms was investigated. The acoustic resistance was shown to increase at low frequencies due to the restrictions.

DD FORM 1 JAN 64 1473

Security Classification

| 14. KEY WORDS | LINK A | | LINK B | | LINK C | |
|---|---|---|---|---|---|---|
| | ROLE | WT | ROLE | WT | ROLE | WT |
| Boundary layer waves | | | | | | |
| Sound propagation | | | | | | |
| Absorber impedance | | | | | | |
| Orifice radiation impedance | | | | | | |
| Acoustic insulation | | | | | | |
| Acoustic properties | | | | | | |
| Acoustic filters | | | | | | |
| Acoustic measurements | | | | | | |
| Gas flow | | | | | | |
| Sound transfiguration | | | | | | |

INSTRUCTIONS

1. ORIGINATING ACTIVITY: Enter the name and address of the contractor, subcontractor, grantee, Department of Defense activity or other organization *(corporate author)* issuing the report.

2*a*. REPORT SECURITY CLASSIFICATION: Enter the overall security classification of the report. Indicate whether "Restricted Data" is included. Marking is to be in accordance with appropriate security regulations.

2*b*. GROUP: Automatic downgrading is specified in DoD Directive 5200.10 and Armed Forces Industrial Manual. Enter the group number. Also, when applicable, show that optional markings have been used for Group 3 and Group 4 as authorized.

3. REPORT TITLE: Enter the complete report title in all capital letters. Titles in all cases should be unclassified. If a meaningful title cannot be selected without classification, show title classification in all capitals in parenthesis immediately following the title.

4. DESCRIPTIVE NOTES: If appropriate, enter the type of report, e.g., interim, progress, summary, annual, or final. Give the inclusive dates when a specific reporting period is covered.

5. AUTHOR(S): Enter the name(s) of author(s) as shown on or in the report. Enter last name, first name, middle initial. If military, show rank and branch of service. The name of the principal author is an absolute minimum requirement.

6. REPORT DATE: Enter the date of the report as day, month, year, or month, year. If more than one date appears on the report, use date of publication.

7*a*. TOTAL NUMBER OF PAGES: The total page count should follow normal pagination procedures, i.e., enter the number of pages containing information.

7*b*. NUMBER OF REFERENCES: Enter the total number of references cited in the report.

8*a*. CONTRACT OR GRANT NUMBER: If appropriate, enter the applicable number of the contract or grant under which the report was written.

8*b*, 8*c*, & 8*d*. PROJECT NUMBER: Enter the appropriate military department identification, such as project number, subproject number, system numbers, task number, etc.

9*a*. ORIGINATOR'S REPORT NUMBER(S): Enter the official report number by which the document will be identified and controlled by the originating activity. This number must be unique to this report.

9*b*. OTHER REPORT NUMBER(S): If the report has been assigned any other report numbers *(either by the originator or by the sponsor)*, also enter this number(s).

10. AVAILABILITY/LIMITATION NOTICES: Enter any limitations on further dissemination of the report, other than those imposed by security classification, using standard statements such as:

(1) "Qualified requesters may obtain copies of this report from DDC."

(2) "Foreign announcement and dissemination of this report by DDC is not authorized."

(3) "U. S. Government agencies may obtain copies of this report directly from DDC. Other qualified DDC users shall request through

_____."

(4) "U. S. military agencies may obtain copies of this report directly from DDC. Other qualified users shall request through

_____."

(5) "All distribution of this report is controlled. Qualified DDC users shall request through

_____."

If the report has been furnished to the Office of Technical Services, Department of Commerce, for sale to the public, indicate this fact and enter the price, if known.

11. SUPPLEMENTARY NOTES: Use for additional explanatory notes.

12. SPONSORING MILITARY ACTIVITY: Enter the name of the departmental project office or laboratory sponsoring *(paying for)* the research and development. Include address.

13. ABSTRACT: Enter an abstract giving a brief and factual summary of the document indicative of the report, even though it may also appear elsewhere in the body of the technical report. If additional space is required, a continuation sheet shall be attached.

It is highly desirable that the abstract of classified reports be unclassified. Each paragraph of the abstract shall end with an indication of the military security classification of the information in the paragraph, represented as *(TS)*, *(S)*, *(C)*, or *(U)*.

There is no limitation on the length of the abstract. However, the suggested length is from 150 to 225 words.

14. KEY WORDS: Key words are technically meaningful terms or short phrases that characterize a report and may be used as index entries for cataloging the report. Key words must be selected so that no security classification is required. Identifiers, such as equipment model designation, trade name, military project code name, geographic location, may be used as key words but will be followed by an indication of technical context. The assignment of links, rules, and weights is optional.